



University of Kerbala
College of Science
Department of Physics

Theoretical study of the electronic and spectroscopic properties for diallyl phthalate

Thesis Submitted to the Council of the College of Science, University of Kerbala in Partial Fulfillment of the Requirements for the Master Degree in Physics

By

Shakir Abdulrazaq Ghulam
B.Sc. University of Baghdad 1983

Supervised by

Assist. Prof Dr. Mohammed Abdulhussain Alkaabi

2022 AD

1443 AH

بِسْمِ اللَّهِ الرَّحْمَنِ الرَّحِيمِ

﴿ وَقُلْ رَبِّ زِدْنِي عِلْمًا... ﴾

صدق الله العلي العظيم

سورة طه: آية - ١١٤

Supervisor Certification

I certify that this thesis, entitled " **Theoretical study of the electronic and spectroscopic properties for diallyl phthalate** "has been prepared under my supervision, by " **Shakir Abdulrazaq Ghulam**" at the department of physics, College of science, University of Kerbala in a partial fulfillment of the requirements for the degree of Master of Science in physics.

Signature:



Name: **Mohammed Abdulhussain Alkaabi**

Title: Assist.professor

Address: Department of physics, college of science / University of Kerbala

Date: 12/5/2022

In view of the available recommendations, I forward this thesis for debate by the examining committee.

Signature:



Name: **Dr. Rajaa A. Madloul**

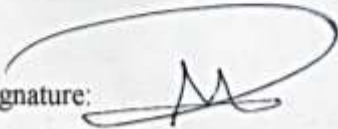
Title: professor


Head of the Physics Department, college of science / University of Kerbala


Date: 15/5/2022

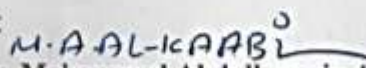
Examination Committee Certification

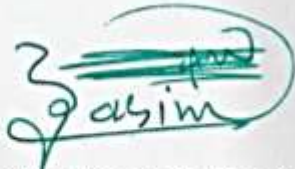
We certify that we have read this thesis entitled " **Theoretical study of the electronic and spectroscopic properties for diallyl phthalate** " as the examining committee, examined the student " **Shakir Abdulrazaq Ghulam** " on its contents, and that in our opinion, it is adequate for the partial fulfillment of the requirements for the Degree of Master in Science of Physics.

Signature: 
Name: **Dr. Mohammed T. Hussein**
Title: professor
Address: Department of physics,
college of science/University of Baghdad
Date: 15/ 5/ 2022
(Chairman)

Signature: 
Name: **Dr. Nagham M. Shiltagh**
Title: Assist professor
Address: Department of physics,
college of science/University of Kerballa
Date: 12/ 5/ 2022
(Member)

Signature: 
Name: **Dr. Rajaa k. Mohammad**
Title: Assist professor
Address: Department of physics,
college of science/University of Kerballa
Date: 15/ 5/ 2022
(Member)

Signature: 
Name: **Dr. Mohammed Abdulhussain Alkaabi**
Title: Assist professor
Address: Department of physics,
college of science/University of Kerballa
Date: 12/ 5/ 2022
(Supervisor)

Signature: 
Name: **Dr. Jasem Hanoon Hashim Al-Awadi**
Title: Assist. professor
Dean of the college of science/ University of Kerballa
Date: 21/6/ 2022

Dedication

To my parents

To my wife

To my children

SHAKIR

Acknowledgment

First, I thank God Almighty for what He has bestowed upon me and given me the ability to complete my thesis.

I would like to express my thanks and appreciation to the Dean of the College of Science and the Head of the Physics Department for their contribution to the completion of this thesis.

I would like to express my great thanks to my supervisor Dr. Mohammed Abdulhussain Alkaabi for his supervision and his valuable directions and opinions.

I thank very much the professors and students of the Physics Department at the College of Science, University of Kerbala for their continuous support and advice and guidance.

Finally, I thank all my family members for their help and encouragement, as well as those who helped me during the preparation of my thesis.

SHAKIR

Abstract

This work investigates the structural and electronic properties of the diallyl phthalate (DAP) monomer. The density functional theory (DFT)/Coulomb-Attenuating Method Beckes three parameter hybrids functional with lee-yang-Parr correlation functional (CAM B3LYP) and Hartree Fock (HF) methods with the 6-311+G (d, p) basis sets are used to treat the many-body system wavefunction. The calculations have been performed and visualized by the Gaussian 09 and Gauss View 06 programs.

The potential energy surface (PES) scan, with the semi-empirical method PM6, was applied on the DAP monomer to get the converged conformer with partial optimization. The full optimization occurred on the converged conformer using the DFT and HF methods. The conformational properties such as bond lengths, bond angles, and the dihedral angles were investigated. For the benzene ring, the average values of the bond lengths of the carbon atoms are 1.389 Å by the DFT and 1.386 Å by the HF, while the calculated value by other researchers is 1.403 Å. The average value of angles, of the benzene ring, is equal to 119.98° by the DFT method, and 120° by the HF method. The results of the aromatic angles show a fair agreement with the standard values.

The electronic energy, natural atomic charge distribution, HOMO and LUMO energies, energy gap, dipole moment, seven global parameters, polarizability, and first-order hyperpolarizability have been studied. The obtained electronic energies are -842.614348 and -837.953983 in the Hartree unit by the DFT and HF methods. Non-uniform charge distribution was observed for both strategies due to the non-zero value of dipole moment (3.3939 and 3.6661 Debye). According to the energy gap value evaluated by the DFT (8.326 eV), the system has more chemical stability compared with the HF value (4.522 eV).

Finally, IR and Raman spectra have been studied and analyzed theoretically by Gauss View 06 and Veda programs. The results obtained by the DFT method revealed a good agreement with the experimental ones for both techniques.

Table of contains

Number	Title	Page
	Abstract	I
	Table of contains	III
	List of Figures	VI
	List of Tables	VIII
	List of Symbols	IX
	Chapter One	
1.1	Introduction	1
1.2	Diallyl Phthalate	2
1.2.1	Structure of Diallyl Phthalate	2
1.2.2	Properties of Diallyl Phthalate	3
1.2.3	Applications of Diallyl Phthalate	5
1.3	Previous Studies	6
1.4	The Aim of the Work	11
	Chapter two	
2.1	Introduction	12
2.2	Schrödinger Equation	12
2.3	Approximation Methods Used in Quantum Computations	14
2.3.1	Molecular Mechanics Methods	15
2.3.2	Ab -initio Methods	15
2.3.2.1	Born-Oppenheimer approximation	16
2.3.2.2	Hartree–Fock approximation	17
	Restricted Hartree-Fock Method (RHF)	18
	Unrestricted Hartree-Fock Method (URHF)	19
2.3.3	Semi-empirical Methods	20

2.3.3.1	Zero-Differential Overlap (ZDO)	20
2.3.3.2	Complete Neglect of Differential Overlap (CNDO)& Intermediate Neglect of Differential Overlap (INDO)	20
2.3.3.3	The Neglect of Diatomic Differential Overlap (NDDO)	20
2.3.3.4	Austin Model 1 (AM1)	20
2.3.3.5	Modified Intermediate Neglect of Differential Overlap (MINDO)	21
2.3.3.6	The Modified Neglect of Diatomic Differential Overlap (MNDO)	21
2.3.3.7	Parametric Model number 3 (PM3)	21
2.3.3.8	Parametric Model number 6 (PM6)	21
2.3.4	Density Functional Theory (DFT)	22
2.4	Hohenberg and Kohn Theorems	24
2.4.1	The First H-K Theorem	24
2.4.2	The Second H-K Theorems	24
2.5	Kohn and Sham	25
2.6	The Exchange Correlation Functionals	27
2.6.1	Local Density Approximation (LDA)	27
2.6.2	Generalized Gradient Approximation (GGA)	27
2.7	Hybrid Functionals	28
2.7.1	Coulomb-Attenuating Method (CAM B3LYP)	29
2.8	Basis Sets	29
2.8.1	Slater Type Orbitals (STO's)	29
2.8.2	Gaussian Type Orbitals (GTO's)	30
2.9.1	Minimal Basis Sets	31
2.9.2	Split-Valence Basis Sets	32
2.9.3	Polarized Basis Sets	32

2.9.4	Diffuse Basis Sets	33
2.10	Electronic properties	34
2.10.1	HOMO, LUMO, and Energy Gap	34
2.10.2	Ionization potential (I)	36
2.10.3	Electron affinity (A)	36
2.10.4	Hardness (η)	36
2.10.5	Softness (s)	37
2.10.6	Electronegativity (χ)	37
2.10.7	Electrophilicity Index (ω)	37
2.9.8	Chemical Potential (ρ)	38
2.10.9	Polarizability and first order hyperpolarizability calculations	38
2.11	Vibrational analysis	39
2.11.1	Infrared Spectroscopy	39
2.11.2	Raman Spectroscopy	40
2.12	Computer used	40
	Chapter three	
3.1	Introduction	41
3.2	Building the monomer of DAP	41
3.3	Potential Energy Surface Scan (PES) of DAP	42
3.4	Full Optimization of the DAP	44
3.5	Structural Properties	45
3.5.1	Bond lengths	45
3.5.2	Bond angles	49
3.5.3	Dihedral angles	51
3.6	Electronic Properties	54
3.6.1	Natural atomic charge distribution	54
3.6.2	HOMO and LUMO	56

3.6.3	Ionization potential (I) and electron affinity(A)	60
3.6.4	Global hardness(η) and Global Softness (S)	60
3.6.5	Electronegativity(χ), Electrophilicity(ω)	60
3.6.6	Chemical potential (ρ)	61
3.6.7	Polarizability and first order hyperpolarizability calculations	62
3.7	Spectroscopy	65
3.7.1	Vibrational Frequencies	65
3.7.1.1	C-H Vibrations	67
3.7.1.2	C=O Vibrations	68
3.7.1.3	=CH Arene Vibrations	68
3.7.1.4	C=C Aromatic Vibrations	68
3.7.1.5	C-O-C Vibrations	69
3.8	Conclusions and future work	75
3.8.1	Conclusions	75
3.8.2	Future works	76
	Reference	77

List of Figures

Figure	Title	Page
1.1	The structure of phthalate in 3D drawing by Gauss View 06	2
1.2	The structure of diallyl	3
1.3	The structure of the diallyl phthalate monomer in 2D	3
1.4	Some applications of the DAP	6
2.1	Shows (a) restricted (R), (b) restricted open shell (RO) and(c) unrestricted (UR) Hartree–Fock methods	19

2.2	HOMO- LUMO and band gap diagram with two interacting molecules	35
2.3	HOMO- LUMO diagram in ground and excited state	35
3.1	The DAP monomer drawing by Gauss View 06 program	42
3.2	Shows (A) Molecule 685 with SC1=180o, SC2=180o, and E = -0.159834 Hartree. (B) Molecule 477 with SC1 = 120o, SC2 = 320o and E = -0.172583 Hartree	43
3.3	Potential energy curve for the angle SC1 (C7-C5-C11-O1)	44
3.4	Potential energy curve for the angle SC2 (C8-C6-C12-O2)	45
3.5	The bond lengths of diallyl phthalate using the (a) DFT and (b) HF method	47
3.6	The linear correlation graph between of the theoretical bond lengths and those calculated in this work	49
3.7	The bond, angle, and dihedral angle diagram	52
3.8	The natural atomic charge distribution for the DAP using (A) DFT (B) HF methods	54
3.9	Natural atomic charge chart analysis at DFT and HF method of DAP molecular	55
3.10	The HOMO and LUMO for the DAP using the DFT method	58
3.11	The HOMO and LUMO for DAP using the HF method	59
3.12	Components and total values of polarizability in CAM B3LYP and HF methods	64
3.13	Components and total values of hyperpolarizability in CAM B3LYP and HF methods	65
3.14	The IR spectrum for the DAP using the CAM B3LYP	70
3.15	The IR spectrum for the DAP using the HF method	70
3.16	Experimental FT-IR spectrum of DAP	71
3.17	The Raman spectrum for the DAP using the CAM B3LYP	72

3.18	The Raman spectrum for the DAP using the HF method	72
3.19	Experimental Raman spectrum of the DAP	73

List of Tables

Table	Title	Page
1.1	Physicochemical Properties of Diallyl Phthalate	4
3.1	The bond lengths (Å) of the DAP using the DFT and HF	48
3.2	The bond angles (degree) of the DAP molecule using the DFT and HF methods	50
3.3	The dihedral angles(degree) of the DAP using the DFT and HF	53
3.4	Natural atomic charge of the DAP using the DFT and HF	56
3.5	HOMO, LUMO, and energy gap for the DAP using the DFT and HF methods	59
3.6	The electronic molecular properties of the DAP monomer using the DFT and HF methods	61
3.7	The dipole moments, polarizabilities, and first hyper polarizabilities of the DAP by the DFT and HF methods	63

List of Symbols

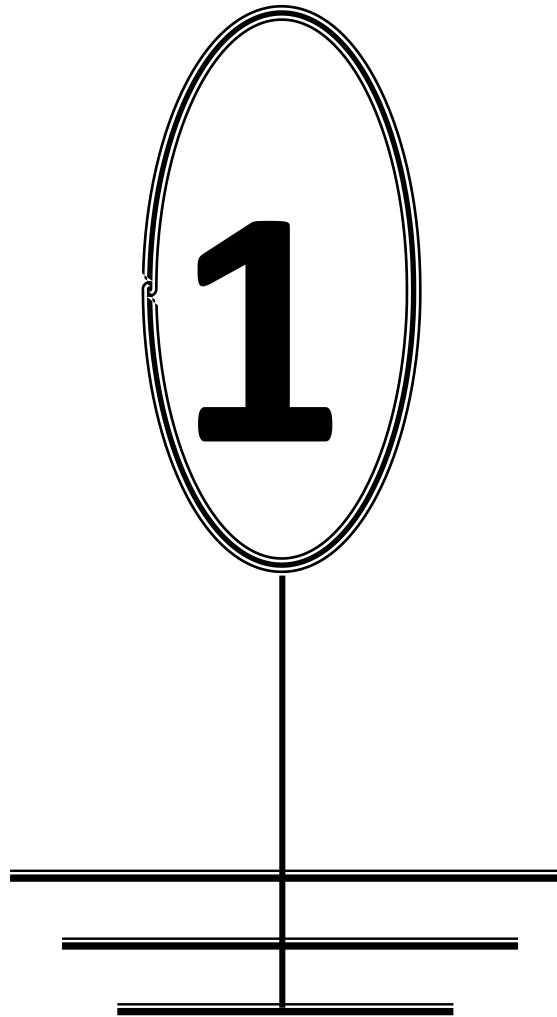
H	Hamiltonian operator
DAP	Diallyl phthalate
$T[\rho]$	Kinetic energy of non-interacting system
$E_{ne}[\rho]$	External energy
$E[\rho]$	Total energy
$J[\rho]$	Electron-Electron repulsion energy
$T[\rho]$	Kinetic energy of non-interacting system
V_{NN}	potential energy operator of nuclei- nuclei
V_H	Hartree potential
r_{ij}	Distance between electron i and j
$\rho(r)$	Electron density
V_{ext}	External potential
V_{ion}	Nuclei potential
V_{XC}	Exchange-correlation potential
E_{XC}	Exchange - correlation energy
HK	Hohenberg-Kohn
ΔE	Energy gap
μ	Dipole moment
I	Ionization energy
A	Electron affinity
χ	Electronegativity
η	Global Hardness
S	Global softness
ρ	Chemical potential
ω	Electrophilicity index
Ψ	Wave function
α	Spin up of electron

β	Spin down of electron
Ψ_i	Spatial wavefunction
ξ	Orbital exponent
MNDO	Modified Neglect of Differential Overlap
MINDO	Modified Intermediate Neglect of Differential Overlap
ZDO	Zero-Differential Overlap
CNDO	Complete Neglect of Differential Overlap
INDO	Intermediate Neglect of Differential Overlap
NDDO	Neglect of Diatomic Differential Overlap
MO	Molecular orbital
AM1	Austin model 1
PM3	Parametric Model number 3
PM6	Parametric Model number 6
HF	Hartree Fock
URHF	Unrestricted Hartree-Fock
RHF	Restricted Hartree Fock
DFT	Density Functional Theory
HK	Hohenberg-Kohn
LDA	Local density approximation
LSDA	local spin-density approximation
GGA	Generalized gradient approximation
LCAO	Linear combination of atomic orbitals
STO	Slater-type orbitals
GTO	Gaussian-type orbitals
HOMO	Highest occupied molecular orbital
LUMO	Lowest unoccupied molecular orbital
FT-Raman	Fourier transform Raman spectroscopy
FT-IR	Fourier transform Infrared spectroscopy

CAM B3LYP	Coulomb-Attenuating Method Beckes three parameter hybrid functional with lee-yang-Parr correlation functional
B3LYP	Beckes three parameter hybrid functional with lee-yang-Parr correlation functional
PES	Potential energy surface scan
MOs	Molecular orbital theories

Chapter One

Introduction



CHAPTER ONE

1.1 Introduction

Polymers have existed in nature since the beginning of time, such as DNA, RNA, proteins, and polysaccharides that play critical roles in plant and animal life. Man has used naturally occurring polymers as materials for decoration, clothing, weapons, shelter, tools, writing materials, and other purposes since the earliest times. However, the origins of today's polymer industry are widely accepted as being in the nineteenth century when significant discoveries concerning the modification of certain natural polymers were made [1].

Modern polymer science has reached a very high level of sophistication. It is now possible to prepare synthetic polymers with well-defined molecular weight as well as relatively easily controlled design of properties [2].

In the last decade, there was the widespread adoption of quantum computing to solve many complex mathematical problems of quantum mechanics, especially after the significant industrial development in the field of quantum mechanics. Based on the computer industry and its software, many researchers have solved the challenges encountered in studying atoms and molecules that were difficult or impossible to examine. This was through hundreds of researches done using computer programs that are still developing continuously.

The theoretical study, the subject of our investigation, is amongst the most critical studies in the current era because it is based solely on theoretical considerations. This study is carried out with the aid of a computer and a specialized program, meaning that it is a simulative experiment. This type of research demonstrated its effectiveness in accurately simulating the material's properties within the limits of a few errors. Our theoretical study will be focused on the diallyl phthalate (DAP) monomer.

1.2 Diallyl Phthalate

1.2.1 Structure of Diallyl Phthalate

The DAP monomer (DAP, $C_{14}H_{14}O_4$) consists of two parts, which are phthalate and diallyl [3]:

First: Phthalate, which in turn consists of a benzene ring connected to two branches of carbon dioxide as shown in the Figure below [4]:

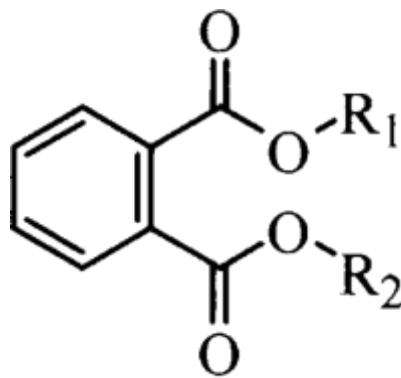


Fig 1.1: The structure of phthalate in 2D [4].

Phthalate is consisting of 8 atoms of carbon, 4 atoms of hydrogen, and 4 atoms of oxygen.

Second: The diallyl consists of two allyl ($CH_2-CH-CH_2$) and each allyl is linked to carbon dioxide.

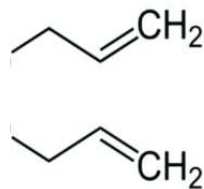


Fig 1.2: The structure of diallyl in 2D [5].

While diallyl is consists of 6 atoms of carbon and 10 atoms of hydrogen. Then, the structure of the diallyl phthalate can be given in the Figure below [6]:

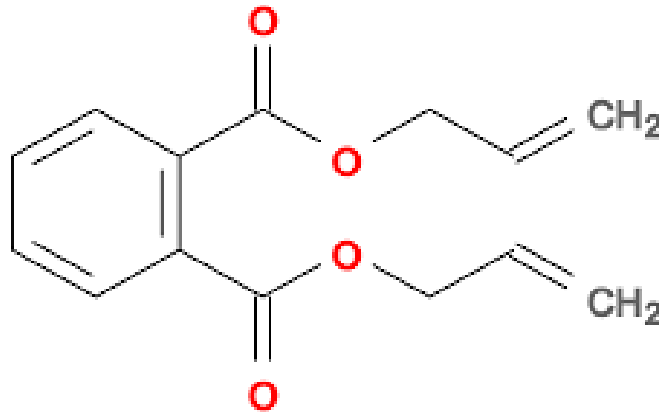


Fig 1.3: The structure of the diallyl phthalate monomer in 2D [6].

1.2.2 Properties of Diallyl Phthalate

DAP is the most commonly used of the allylic esters, which are a branch of the polyester family and among the most versatile of the thermosetting resins. It is chosen for applications that require outstanding dimensional stability, ease of molding, low water absorption, and excellent electrical properties [7, 8].

There are only two resins that are clear, easily polymerizable, and have a high refractive-index: DAP and styrene. Besides having a high refractive index, DAP has other advantages; such as a good colour, excellent heat resistance and form stability at elevated temperatures, good hydrolytic stability, excellent electrical properties, low vapour pressure, and is free from handling hazards [9].

Moreover, it had many mechanical properties: Excellent strength in compression, thin wall strength, impact resistance, for applications subjected to sudden extreme jolts and severe stresses, in addition to an unaffected performance by high ambient humidity.

Despite these excellent properties, the usage of DAP resins is limited because of their poor adhesive properties to various metals. There are a few approaches to the improvement of adhesive properties for DAP resins in comparison with those of epoxy resins and polyimides. To improve their adhesive properties, DAP resins have been blended with epoxy resins superior in adhesive strength to metal. The peel strength of copper foil on the DAP resin increased through blending with epoxy resin; however, the heat resistance of the DAP resin that was blended with epoxy resin decreased markedly [10, 11]. The physicochemical properties are listed in Table below:

Table 1.1 Physicochemical Properties of Diallyl Phthalate [3].

Identification	Information
Chemical Name	Diallyl phthalate
Synonyms	1,2-Benzenedicarboxylic acid, di-2-propenyl ester, Allyl phthalate, Dapon 35, Dapon R; Di-2-propenyl 1,2- benzene dicarboxylate; Phthalic acid, diallyl ester; o- Phthalic acid, diallyl ester; 1,2 Benzene dicarboxylic acid, 1,2-di-2-propen-1-yl ester
CAS Number	131-17-9
Chemical Formula	$C_{14}H_{14}O_4$
Physical State	Liquid
Colour	Colourless
Melting Point	-70 ° C
Boiling Point	158 -165° C @ 4 mm Hg
Vapour Pressure	1.16E-03 mm Hg @ 25°C
Water Solubility	182 mg/L @ 20°C
Molecular Weight	246.26 g/mole
Flashpoint	166°C

1.2.3 Applications of Diallyl Phthalate

One of its important applications of the DAP is a track detector with exceptional properties: its selective registration of heavy charged particle tracks, like FTs, and insensitivity to light particles such as α -particles, distinguishes it from other plastic track detectors. It's FTs are resistant to heating for 1 h at 240 C° 1 MGy γ -doses. Moreover, the appropriate etching solutions produce large elliptic track openings that are suited for automated track counting [12].

At present, Poly diallyl Phthalate (PDAP) is mainly used for electrical and electronic devices as well as for the production of thermoforming compounds due to its good flowability, good dimensional stability, and its electrical and thermal properties [13].

Because of its outstanding mechanical properties, it is used for high-volume forming compounds, specialty coatings, and for decorative laminated sheets [14]. In some molding compounds, the addition of inorganic materials to the prepolymer increases the mechanical performance of these thermosetting polymers after exposure to high humidity for various periods of time. Some of these application are shown in the Figure 1.4 [13]:



Fig 1.4: Some applications of the DAP: (a) laminated decorative sheet (b) advanced electronic devices (c) electrical devices and (d) light emitting diodes (LEDs) [13].

1.3 Previous Studies

In this section, we will exhibit some studies that achieved to the diallyl phthalate experimentally and theoretically, as follow:

- **Haward** (1954) [15], used a simple statistical model to study the polymerization of diallyl phthalate. The possibility of intramolecular response is calculated for the polymerizing diallyl phthalate molecule. The outcome is consistent with Simpson's experimental findings, in which a significant opportunity was discovered. Haward used the statistical model to calculate the probability by assigning bond lengths and angle values.

- **Heydel, Cassagnau, and Michel** (1999) [16], studied the bulk crosslinking of diallyl phthalate monomers. Dynamic mechanical analysis and infrared spectroscopy were used to investigate the radical crosslinking of ortho diallyl phthalate. Rheological measurements calculated the effective formation of the network band, whereas infrared spectroscopy measured uninteracted allele bonds. As a result, infrared spectroscopy did not represent a lattice but rather the disappearance of a double bond.

- **Tsuruta** (2000) [17], investigated diallyl phthalate (DAP) and allyl diglycol carbonate (CR-39). Under the same polymerizing conditions, DAP and CR-39 mixtures were cast into plates. Alpha particles, fission fragments, and fast neutrons were used to irradiate the plates. According to the findings, the pure DAP plate has a high detection efficiency for fission fragments but is insensitive to alpha particles and fast neutrons. Pure CR-39 plate, on the other hand, helped detect alpha-particles and fast neutrons due to its high detection efficiency and sensitivity, as well as its short etching time. It was discovered that DAP and CR-39 copolymers exhibited intermediate properties between DAP and CR-39 resin.

-**T. Yoshioka *et al.*** (2006) [18], assessed the radioactivity of neutron-irradiated materials used for fission-track (FT) dating. The effective dose rates and specific activities of neutron-irradiated minerals (zircon, apatite, and sphene), a muscovite detector, and a diallyl phthalate (DAP) resin detector were measured. Except for DAP, all materials had much higher specific activities after irradiation. Their activities continued for a long time because they contained several isotopes with long half-lives, such as Sc-46 and Ta-182. In contrast, no radioisotopes were detected in DAP, except for a small portion of Br-82, whose activity was found to be very much lower than that of the previously mentioned radioisotopes, decreasing to background levels after several days.

-**Xu *et al.*** (2008) [14], performed the bulk polymerization of diallyl phthalate (DAP) at high temperatures (190 °C) without the use of an initiator, and the reaction was stopped before the gelation point to obtain the DAP prepolymer. The ultrasonic separation product is characterized by infrared spectroscopy (IR), gel permeation chromatography (GPC), and iodine number measurement. Infrared spectroscopy showed that the wavenumbers of the spectra were: CH stretching vibration on benzene = 3074/3076 frequency/ cm^{-1} , C=O stretching vibration = 1720 frequency/ cm^{-1} , =CH stretching vibration on arene = 1649 frequency/ cm^{-1} , C=C on benzene = 1599, 1579 frequency/ cm^{-1} .and C–O–C = 1282, 1123, 1069/1283, 1125, 1070 frequency/ cm^{-1} .

- **Gerbaux P** (2010) [19], studied dimethyl phthalate (DMP), and it's analogous using density functional theory with the hybrid functional B3LYP and 6-311++G (d, p) basis set. The bond lengths, harmonic vibrational frequencies, and zero-point energies were performed. From the result of optimization, the bond lengths of the benzene ring range from 1.38 Å to 1.40 Å, C-O bond is 1.34 Å, C=O bond is 1.21 Å, C-H bond is 1.128 Å, and the C-C bond length for allyl is 1.49 Å. All calculations were achieved using the Gaussian 03 software.

- **Jeelani, Cardelino, and Ibeanusi** (2011) [20], used DFT and Mass Spectroscopy to study the energetic of the fragmentation mechanism of phthalate. Analysis of phthalates has been pronounced via way of means of mass spectrometric approaches. DFT was used to find geometries and energetics of the monomer. The hybrid functional B3LYP with basis sets 6-311 G (d, p) was used. All optimized geometries have been subjected to vibrational frequency evaluation to ensure they corresponded to minima without imaginary frequency. Natural bond orbital analysis was done to calculate atomic charges and spin densities. Zero-point energies had been received from harmonic frequency calculations without scaling. The translational, rotational, and vibrational contributions to the

enthalpy and entropy had been evaluated the usage of rigid-rotor harmonic oscillation approximations.

- **Yadav and Pandey** (2012) [21], studied the stability, structural and electronic properties of 19 small-group $Zn_m Se_n$ ($m + n = 2-4$) nanoclusters. The B3LYP-DFT/6-311G (3df) method was used to improve the geometries of nanoclusters. Zero-point energy was calculated, which was ignored by other workers. The binding energies, HOMO–LUMO energy gaps and the bond lengths for all optimized nanoclusters were obtained. Moreover, the adiabatic and vertical ionization potentials, electron affinity, dipole moment and charge on atoms were investigated for the most stable nanoclusters.

- **Şen *et al.*** (2014) [22], examined the allyl diglycol carbonate (CR-39) most used in the manufacture of eyeglass lenses theoretically. The structure monomer of CR-39 was optimized by density functional theory using the method B3LYP with basis set STO-3G without determining any symmetry for the title molecule. The non-linear optical features were calculated at the same level, and the title compound showed a good second-order non-linear optical feature. Besides that, the energies of frontier molecular orbital (HOMO and LUMO), bond lengths, total energy, zero-point energy, dipole moment and entropy of CR-39 monomer were studied.

-**Ridha, Saleh, and Askar** (2015) [23], calculated the geometrical parameters, electronic absorption maximum wavelengths, vibrational frequencies, frontier orbitals HOMO-LUMO, dipole moment, total energy and energy difference of Nitron using density functional theory method and B3LYP with basis set 6-311 G (d, p). The solid-phase Fourier Transform-Infrared FT-IR spectrum of the title compound was recorded. Finally, the comparison between the experimental data and the calculated results showed good agreement.

- **Xu *et al.*** (2019) [24], used DFT methods to find the energy values of five PAEs such as DMP, DEP, DPP, DAP and DBP. The global minimum energy was performed by TURBOMOLE software. The molecular descriptors of sub-structures of PAE molecules were calculated by Gaussian 09 software and Dragon software (6). These descriptors include partial atomic charges, the energy of a higher occupied molecular orbital, a lowest unoccupied molecular orbital, chemical hardness, chemical smoothness, electronegativity, electrophilic index, polarizability, electron affinity, bond arrangement, and dipole moment.

- **Nageswara *et al.*** (2019) [25], studied computational methods of dimethyl phthalate to evaluate the electronic properties of molecular systems. Total chemical quantum calculations were carried out in DFT and HF methods with basis set 6-311++G (d, p) using the Gaussian09 software program. The results obtained using the DFT method of the structure geometry, atomic charges, vibrational frequencies, thermodynamics properties and dipole moment have good agreement with experimental ones. Energy as a function of SC1 (C₈-C₁₀-C₁₁-O₁₂) and SC2 (C₁-C₂-O₅-C₉) was achieved using the method of the AM1.

The bond length C-O is found to be greater than the bond length C=O. The values of bonds C₂=O₆ and C₁₁=O₁₃ were found to be 1.209 Å. The results showed that the value of HOMO is -7.5639 eV, while the value of LUMO is -2.2417 eV, and the energy gap is 5.322 eV.

1.4 The Aim of the Work

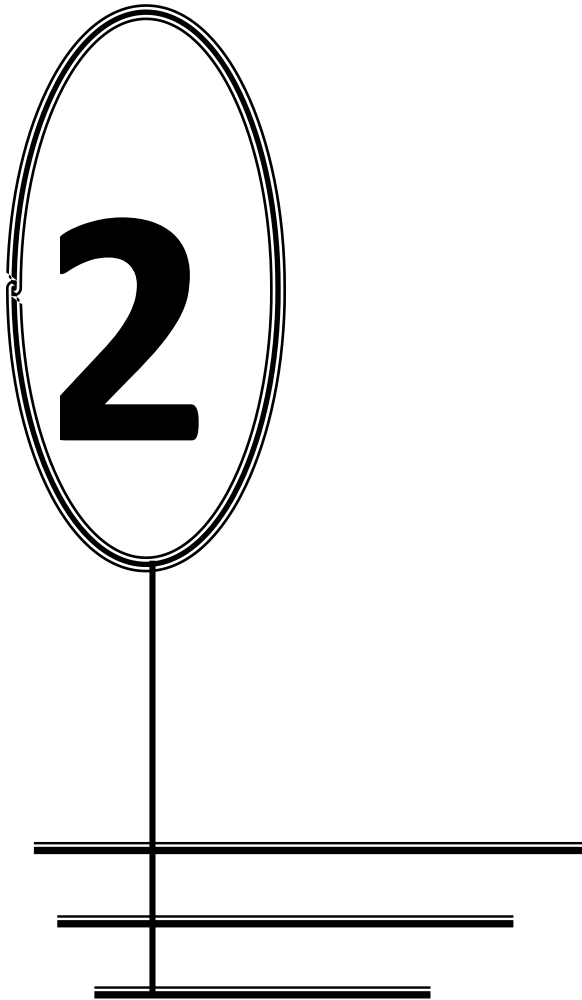
The work aims to study the structural properties of diallyl phthalate such as bond length, bond angle and dihedral angle. Moreover, electronic properties such as natural atomic charge distribution, dipole moment, polarizability and Hyperpolarizability, ionization potential, electronegativity, chemical potential, electron affinity, hardness, softness, and electrophilicity index will be investigated. All calculations are carried out using Gaussian 09 software programs and GaussView6 by using the density functional theory with hybrid method CAM B3LYP.

The investigated properties extend to the energy gap, the difference between (HOMO) highest occupied molecular orbital and (LUMO) lowest unoccupied molecular orbital. In addition to vibrational properties, including (IR) infrared spectroscopy and Raman spectroscopy.

Chapter Two

Theoretical

Methods



CHAPTER TWO

THEORETICAL METHODS

2.1 Introduction

Many theories have emerged to investigate and comprehend the electronic properties of molecules; density functional theory is one of the most prominent and widely used of these theories. DFT is now broadly recognized as a powerful method for computing the quantum state of atoms, molecules, and solids, as well as ab-initio molecular dynamics. In 1927, shortly after the establishment of quantum mechanics, Thomas and Fermi proposed an initial and approximate form of density functional theory. Later, Hohenberg, Kohn, and Sham produced a density functional theory of the quantum ground state that was superior to both Thomas-Fermi and Hartree-Fock theories, opening up a wide range of applications for actual physical systems [26] .

This chapter will define and explain the Schrödinger equation, molecular computational methods, electronic properties. More attention will be paid to the HF, semi-empirical, and Density functional theory methods, which have been used to find the calculations of this work.

2.2 Schrödinger Equation

As per classical mechanics, a system of interacting particles has a total energy that is equal to the sum of kinetic energy and potential energy; it is given by [27]:

$$E = T + V \quad (2-1)$$

The right way to explain the wave character of particles, according to Schrödinger, is to exchange the classical kinetic and potential energy.

$$\{\hat{T} + \hat{V}\}\psi = \hat{E} \psi \quad (2-2)$$

or

$$\hat{H} \psi = \hat{E} \psi$$

Where ψ is the eigenfunction that describes the electron motion of the system, \hat{V} is the potential energy operator, and \hat{E} is the eigenvalue of the Hamiltonian \hat{H} [4].

It is helpful to take a step back and recall some fundamental quantum physics to understand what density-functional theory is about. In quantum mechanics, we discover that a wave function of a system contains all of the information we may know about it. This wave formula is obtained nonrelativistically using Schrodinger's equation, which for a single electron travelling in a potential $V(r)$ can be written as [28]:

$$\left[\frac{-\hbar^2}{2m} \nabla^2 + V(r) \right] \psi(r) = E \psi(r) \quad (2-3)$$

The total Hamiltonian of the system, which includes n electrons and N nuclei, can be expressed as follows:

$$\hat{H} = \hat{T}_N(R) + \hat{T}_e(r) + \hat{V}_{eN}(r, R) + \hat{V}_{NN}(R) + \hat{V}_{ee}(r) \quad (2-4)$$

The kinetic energy operators of nuclei and electrons, respectively, are $\hat{T}_N(R)$ and $\hat{T}_e(r)$. The potential energy operators of electron–nuclei, nuclei–nuclei, and electron–electron are $\hat{V}_{eN}(r, R)$, $\hat{V}_{NN}(R)$, and $\hat{V}_{ee}(r)$, respectively. R stands for nuclear coordinates, whereas r stands for electron coordinates.

So, equation (2-4) can be given by [4]:

$$\begin{aligned} \hat{H} = & -\frac{\hbar^2}{2} \sum_{I=1}^N \frac{\nabla_I^2}{M_I} - \frac{\hbar^2}{2} \sum_{i=1}^n \frac{\nabla_i^2}{m_i} - \sum_{I=1}^{N-1} \sum_{i=1}^n \frac{e^2 Z_I}{r_{Ii}} + \sum_{I=1}^{N-1} \sum_{J=I+1}^N \frac{e^2 Z_I Z_J}{R_{IJ}} \\ & + \sum_{i=1}^{n-1} \sum_{j=i+1}^n \frac{e^2}{r_{ij}} \end{aligned} \quad (2-5)$$

Where: M is the mass of the nucleus, m is the mass of the electron, e is the charge of the electron, Z_I and Z_J are the charges of the nucleus of atoms I and J ,

r_{Ii} is the distance between nuclei I and electron i , R_{IJ} is the distance between nuclei I and J , and r_{ij} is the distance between electrons i and j .

The energy function includes three terms, the kinetic energy, the interaction with the external potential, and the electron-electron interaction, as can be seen from the Schrodinger equation.

Equation (2-5) can be write using an atomic unit value (e^2 , \hbar^2 and $m=1$) as follow:

$$\hat{H} = -\frac{1}{2} \sum_{I=1}^N \frac{\nabla_I^2}{M_I} - \frac{1}{2} \sum_{i=1}^n \frac{\nabla_i^2}{m_i} - \sum_{I=1}^{N-1} \sum_{i=1}^n \frac{Z_I}{r_{Ii}} + \sum_{I=1}^{N-1} \sum_{J=I+1}^N \frac{Z_I Z_J}{R_{IJ}} + \sum_{i=1}^{n-1} \sum_{j=i+1}^n \frac{1}{r_{ij}} \quad (2-6)$$

The finding of molecular eigenfunctions has long been a fundamental difficulty in quantum mechanics. Only the hydrogen atom and the molecular hydrogen ion have exact analytical solutions to the Schrodinger equation. Eigenfunctions can only be produced in an approximate form for more complex systems using approximate methods [29].

2.3 Approximation Methods Used in Quantum Computations

- Molecular Mechanics Methods (MM).
- Ab -initio Method.
- Semi-Empirical Methods (SE).

2.3.1 Molecular Mechanics Methods (MM)

The application of Newtonian mechanics to describe molecular systems is referred to as MM. In molecular structure refinement, molecular dynamics simulations, and ligand docking simulations, molecular mechanics techniques are commonly used. Small molecules, huge biological systems, and material assemblies with thousands to millions of atoms can all be studied using MM. Each atom is simulated as a single hard spherical particle with a radius and a constant net charge in all-atomistic MM methods. Furthermore, bond interactions are considered as "springs", with equilibrium distances and harmonic force constants equivalent to the experimentally determined or computed bond lengths and vibrational frequencies [30].

The MM method calculates energy depend on improving or changing the spatial structure of the studied compounds to reach the lowest possible energy. The particles are treated as if they are balls connected to each other by means of springs that do not take electrons into account, and to calculate the energy value, one must identifying the real bond length between each two atoms and the angle between them, as well as the tensile and bending energy of the new bond[31] .

2.3.2 Ab -Initio Methods

Ab-initio is a Latin term that means "from first principles" or "from scratch," and it refers to computations that are made entirely from theoretical principles without the use of empirical evidence. The majority of the time, this relates to a rough quantum mechanics computation. Mathematical approximations are commonly used, such as employing a simplified functional form of a function or finding an approximate solution to a differential equation [32].

The most frequent ab-initio calculation is a Hartree-Fock HF computation, with a central field approximation as a first approximation. The energies from HF computations are usually more significant than the exact energy. They tend to a

specific value known as the Hartree Fock limit, and this is due to the central field approximation. In HF calculations, the second approximation is that the wavefunction must be characterized by some functional form, which is exact for just a few electron systems.

On the other hand, new users are faced with questions about which basis set to employ, whether or not electron correlation corrections are required, and other related issues. The goal of ab initio Molecular Orbital Theory (MOT) is to give the necessary knowledge and answer these questions. It starts with a basic introduction to ab initio theory and computational methodologies [33].

Computer programs are also employed to perform the necessary calculations to solve the Schrödinger equation due to the enormous number of particles in the systems. For complex systems, these calculations include a large number of complicated integrals. All of these integrals can be solved without rounding using ab-initio arithmetic methods. For small and medium-sized systems, ab-initio methods are the most reliable, but they are time-consuming for large systems [4].

2.3.2.1 Born-Oppenheimer Approximation

Although a molecule contains both nuclei and electrons, the nuclear and electronic motions can be considered independently since nuclei are substantially heavier than electrons and so have greater restrictions on their mobility. The Born-Oppenheimer approximation was formulated in 1927 to describe the separation of nuclear and electronic motion using a precise but rather complex mathematical analysis [29]. So, the molecule wave function can be divided into:

$$\Psi(r, R) = \Psi_e(r, R)\Psi_N(R) \quad (2-7)$$

Where Ψ_e and Ψ_N can be found independently by solving two Schrödinger equations.

The kinetic energy of nuclei and the potential energy of nuclei-nuclei could be removed from the Hamiltonian operator, resulting in the following simplified operator:

$$H = T_e + V_{ee} + V_{eN} + V_{NN} \quad (2-8)$$

Only three energy operators remain in the simple equation. T_e stands for electron kinetic energy, V_{ne} for electron-nuclear interaction energy, and V_{ee} for electron-electron interaction energy. The system may be described as all electrons moving in a fixed-position potential field of nuclei. It is now required to state that the Schrödinger equation is simplified by the Born-Oppenheimer approximation, and that this consistent approximation is the first stage in reaching the decision. The new wave function is based on the electron coordinates of the system, and the new form of Schrödinger's equation is still a system with many bodies. The electrons are interacting with each other, making the problem more complex to solve. As a result, more approximations are required for decision-making [34].

2.3.2.2 Hartree–Fock Approximation

Hartree Fock theory [35, 36] is one of the most basic wave function theories. The central field approximation is the basic approximation, which implies that the electron repulsion potential is derived using the integral of all electrons. As a result, net electron and electron repulsion is obtained, which ignores the effects of electrons between them. Thomas and Fermi proposed a computational model for determining the energy of atoms by approximating the distribution of electrons in an atom the same year as the Hartree technique, in 1927 [37]. Hartree offered his approach to the Schrödinger equation solution. He assumed that an n -electron system's overall wavefunction may be represented as a product of single electron functions $\psi_1, \psi_2, \dots, \psi_n$

$$\Psi(1,2, \dots, n) = \psi_1(1)\psi_2(2)\psi_3(3) \dots \dots \psi_n(n) \quad (2-9)$$

The product of all individual electron functions (orbital) is $\Psi(1,2, \dots, n)$. Until now, the Pauli Exclusion Principle has not taken into account the spin of electrons [38].

The quantum numbers of two electrons cannot be the same. Alternatively, an orbital can hold a maximum of two electrons, and the electron spins are coupled. The interchange of coordinates between two electrons should be asymmetric. As a result, a Slater determinant can express the total wave function of many-electron systems.

Fock replaced the total wave function $\Psi(1,2, \dots, n)$ of Hartree by a Slater determinant. So, the wave function in the Hartree-Fock approximation can also be expressed as a determinant, known as the Slater determinant. The spin of electrons obeys Pauli's exclusion principle in this determinant. The electrons can have the values $(+\frac{1}{2})$ and $(-\frac{1}{2})$ for spin up (α) and spin down (β). According to Slater determinant, the wave function of a system consisting of N electrons can be written as [39]:

$$\Psi(r_1, r_2, \dots, r_N) = \frac{1}{\sqrt{N!}} \begin{vmatrix} \psi_1(r_1) & \psi_2(r_1) & \dots & \psi_N(r_1) \\ \psi_1(r_2) & \psi_2(r_2) & \dots & \psi_N(r_2) \\ \vdots & \vdots & & \vdots \\ \psi_1(r_N) & \psi_2(r_N) & \dots & \psi_N(r_N) \end{vmatrix} \quad (2-10)$$

ψ is the spin-orbit electronic wave function and $\frac{1}{\sqrt{N!}}$ is the normalization factor. The Schrödinger equation for a quantum system with n electrons and an N nucleus can be solved using this method.

- **Restricted Hartree-Fock Method (RHF)**

A variation on the HF method is the manner in which orbitals are built to reveal paired or unpaired electrons. The same orbital spatial function can be utilized for both the α and β spin electrons in each pair if the molecule has a singlet spin. This way is called the restricted Hartree-Fock method (RHF) [40], see Figure. 2.1.

- **Unrestricted Hartree-Fock Method (URHF)**

There are two methods for creating HF wave functions from molecules with unpaired electrons. One method is to use two completely distinct sets of orbitals for the α and β electrons. This is called an unrestricted Hartree-Fock wave function (UHF). This means that the spatial distribution of coupled electrons will be different [40]. In this method, there are two sets of spatial orbitals - one with up-spin (α) electrons and the other with spin-down (β) electrons. This leads to two sets of orbitals as shown in Figure. 2.1.

The restricted open shell Hartree-Fock method is another method for creating wave functions for open-shell molecules (ROHF). The paired electrons in this approach share the same spatial orbital. The ROHF technique is more complex to adopt than UHF, and it may take a little longer CPU time to run [40].

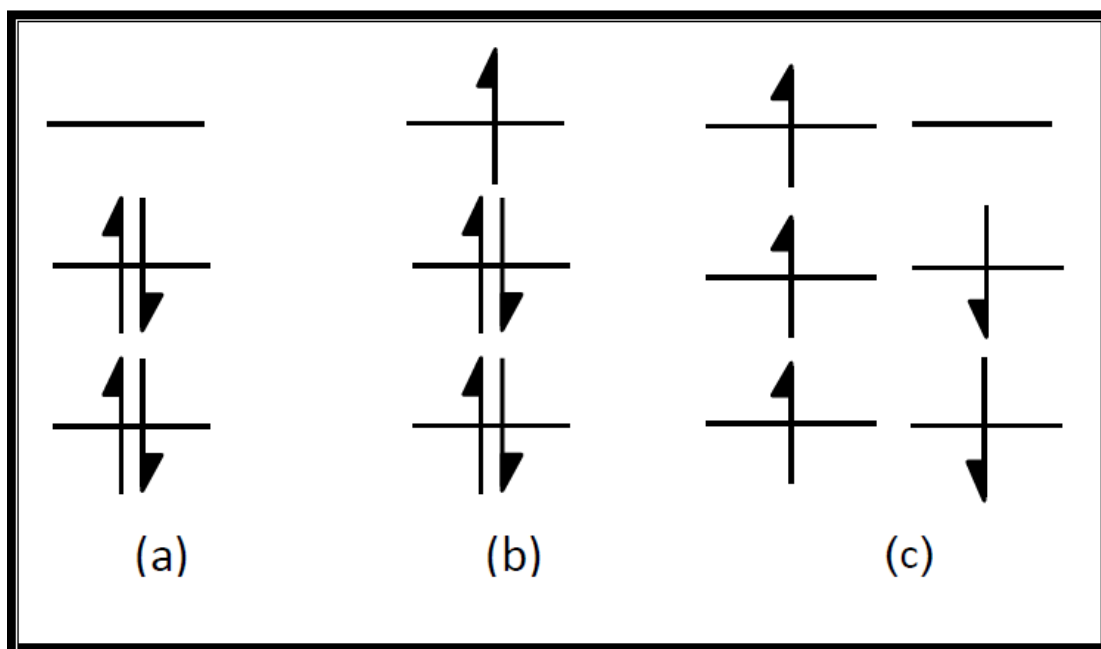


Fig 2.1: Shows (a) restricted (R), (b) restricted open shell (RO) and(c) unrestricted (UR) Hartree-Fock methods [41].

2.3.3 Semi-Empirical Methods

Semi-empirical approaches in solid-state chemistry have a long and productive history, spanning several decades. When computational capabilities did not allow for more precise procedures, approximate molecular orbital simulations lay the groundwork for later ab initio methods. As computers become more powerful, it is wondered if semi-empirical methods are still necessary [42].

Semi-empirical methods have been classified into several methods [40]:

2.3.3.1 Zero-Differential Overlap (ZDO)

This method served as the foundation for most semi-empirical methods. Interference between electrons in various orbitals was assumed to be zero.

2.3.3.2 Intermediate Neglect of Differential Overlap (INDO) & Complete Neglect of Differential Overlap (CNDO)

INDO is a semi-empirical quantum chemistry approach that is a progression of John Pople's complete neglect of differential overlap (CNDO/2). It uses zero-differential overlap for two-electron integrals, similar to CNDO/2, but not for integrals over orbitals centered on the same atom.

2.3.3.3 The Neglect of Diatomic Differential Overlap (NDDO)

It is a two-atomic differential interference neglect approximation [43].

2.3.3.4 Austin Model 1 (AM1)

It is a common rapid method for modelling organic compounds because, unlike other quasi-experimental methods, it produces more accurate findings. It is employed in molecular engineering as well as to strengthen activation energies. AM1 is more precise for hydrogen bond energies [44].

2.3.3.5 Modified Intermediate Neglect of Differential Overlap (MINDO)

In 1969, M.J.S. Dewar and Bird proposed modified Neglect approximation methods for diatomic Overlap of three types [MNDO1, MNDO2, MNDO3], where the experimental results are used to calculate the heat of production [40].

2.3.3.6 The Modified Neglect of Diatomic Differential Overlap (MNDO)

Dewar and Thail published their modified neglect approximation approach for differential interferences in 1977. This method is based on the NDDO method, which is more precise than the INDO method adopted in MINDO/3 [40].

2.3.3.7 Parametric Model number 3 (PM3)

PM3 is stronger than the NDDO model that is still commonly used today. Although this method employs nearly the same equations as AM1, it is more accurate, particularly when estimating hydrogen bond angles [44]. It is also used to compute total energy, structural properties, and formation heat. Some PM3 features may cause abnormal behaviors still being investigated [40, 45].

2.3.3.8 Parametric Model number 6 (PM6)

This method was improved since it allowed for the use of (d) orbitals, which allowed it to be applied to transition metals and broadened the scope of the study to include a wide range of compounds [46].

2.3.4 Density Functional Theory (DFT)

DFT is a method that has gained popularity since the late 1980s and continues today. A functional function is described as a function whose solution results in another function, that is, the function of the function [2].

This method, like the ab initio and semi-empirical methods, is based on the Schrödinger equation. However, instead of the wave function, it employs the electronic density function [47, 48]. The basic idea behind density functional theory is that the energy of the system can be given by its density:

$$E = E(\rho) \tag{2-11}$$

Using an electronic density function, the DFT theory reformulates the quantum difficulties and converts them from a many-particle to a single-particle system problem. The latter can only be calculated with three variables and thus reduces the number of variables used in the calculation as a basis for measurement.

DFT is one of the most well-known and widely used quantum mechanical methods to matter. It is now routinely used in chemistry and physics to calculate, for example, the binding energy of molecules and the band structure of solids. First applications applicable to fields usually believed to be more distant from quantum mechanics, such as biology and mineralogy, are arising. DFT has been used to investigate superconductivity, atoms at the focus of intense laser pulses, relativistic effects in heavy elements and atomic nuclei, classical liquids, and alloy magnetic characteristics [4].

The ground state energy of a system may be given by the following equation:

$$E_{\text{DFT}}[\rho] = T[\rho] + J[\rho] + E_{\text{ne}}[\rho] + E_{\text{XC}}[\rho] \tag{2-12}$$

$T[\rho]$ is the kinetic energy of a non-interacting system, $J[\rho]$ is the electron-electron repulsion energy, $E_{\text{ne}}[\rho]$ is the External potential, and $E_{\text{XC}}[\rho]$ is the exchange-correlation energy functional.

The exchange and correlation function $E_{XC}[\rho]$ contains a set of unobtainable information, is calculated by summing both the exchange function E_X and the correlation function E_C as follows:

$$E_{XC} = E_X + E_C \quad (2-13)$$

Hohenberg, W. Kohn, and L. Sham developed DFT, which showed two basic hypotheses on which the DFT is established. The theory enables the characteristics of a many-body system's base state [49-55]. It is used to bulk materials as well as more complicated structures like proteins and functional nanostructures. In atomic, molecular, solid state, and nuclear physics, density functional techniques have become an important tool in the treatment of many-body issues. The successful implementation to stationary systems has lately inspired renewed interest in using density functionals to solve time-dependent problems: The dynamical response of inhomogeneous metallic systems, atomic and nuclear scattering processes, light absorption in atoms, and atomic and nuclear scattering processes have all been successfully explored [56].

The electron density $\rho(\vec{r})$, at a given point in space is a quantity that is directly related to probability. The DFT permits a simpler electron density to be used instead of the complex electron wavefunction N and the related Schrödinger equation.

The total number of electrons is determined by the electron density integral, as in the following equation [57]:

$$\int \rho(\vec{r})d\vec{r} = N \quad (2-14)$$

The relation between the many-electron wavefunction Ψ_e and $n(\vec{r})$ can be given by:

$$\rho(\vec{r}) = N \iint \dots \int \Psi_e^*(\vec{r}_1, \vec{r}_2, \dots, \vec{r}_n)\Psi_e(\vec{r}_1, \vec{r}_2, \dots, \vec{r}_n)d\vec{r}_1 d\vec{r}_2 \dots d\vec{r}_n \quad (2-15)$$

From calculating the entire wave function to the Schrödinger equation, a function of the $3N$ coordinates, an electron density with only three coordinates carries a massive quantity of physically observable information. The application of electron density functions gave rise to the functional name density theory.

2.4 Hohenberg and Kohn (H-K) Theorems

The ground state of a many-electron system can be determined from the ground state electron density $\rho(r)$, as Hohenberg and Kohn demonstrated in 1964. The Hohenberg and Kohn's two theorems are:

2.4.1 The First H-K Theorem

The ground state features of a multi-electron system are determined directly by an electron density that relies just on three spatial coordinates, according to Hohenberg and Kohn's first theorem (r has three variables). They stated their first theorem: consider: an arbitrary number of electrons enclosed in a large box and transferring through the external potential and the mutual repulsion of Coulomb [37, 58]. The Hamiltonian has the following form:

$$H = T + V + U \quad (2-16)$$

where T represents the N -electron kinetic energy, V represents the N -electron potential energy from the external field, and U represents the electron-electron interaction energy [58].

2.4.2 The Second H-K Theorems

Hohenberg and Kohn, in their second theorem, describe an energy functional for the system in terms of electron density. They show that the ground state energy may be determined by taking the minimum of the energy functional according to the electron density [37]:

$$E(\rho_0) = \text{Min } E(\rho) \quad (2-17)$$

2.5 Kohn and Sham Theory

The theory of Hohenberg and Kohn presented the possibility of functional density and demonstrated the existence of a unique interrelationship between the ground state of density and ground energy. But it did not provide any proof of the functional function that leads to ground energy or how to obtain it, which was discovered one year later by Kohn and Sham [50].

Instead of limiting device resources, the Kohn-Sham method is the most often employed technique. In 1965, Kohn and Sham produced a work that condensed the multi-electron problem into a problem of non-interaction electrons with an efficient potential, just one year after Hohenberg and Kohn's key paper. This potential includes the external potential as well as the effects of electron Coulomb interactions, such as exchange.

Kohn and Sham developed the DFT theory by simulating the Schrödinger equation to find the wave functions that correspond to the lowest total energy value. Variations in the electron density of a system undergoing structural transformation or chemical reaction were utilized to deduce the forces driving the transformation or reaction. Indeed, since the advent of quantum mechanics, electron density has been regarded as one of the most important descriptors of a system of electrons and nuclei. The total energy of a system can be considered as a functional of the electron density, according to the Hohenberg–Kohn theorem 1. The Kohn–Sham theory 2 allows us to generate the real ground-state electron density of an N-electron system from the N one-electron orbitals of the lowest-energy of a particular independent electron system, which is summarized in the equation below [59]:

$$H_{ks}\psi_i = E_i\psi_i \quad (2-18)$$

And therefore

$$\left[\frac{-\hbar^2}{2m} \nabla^2 + V_{ion}(\vec{r}) + V_H(\vec{r}) + V_{xc}(\vec{r}) \right] \psi_i(\vec{r}) = \varepsilon_i \psi_i(\vec{r}) \quad (2-19)$$

$\psi_i(\vec{r})$ is the electron wave function. It represents the mathematical expression of the de Broglie wave associated with the particle, ε_i is the particle total energy.

While the effective potential of the system can be given by:

$$V_{eff} = V_{ion}(\vec{r}) + V_H(\vec{r}) + V_{xc}(\vec{r}) \quad (2-20)$$

Or

$$V_{eff} = V_H + V_{xc} + V_{ext} \quad (2-21)$$

Where $V_{ion}(\vec{r})$ (V_{ext}) is the nuclei potential, and $V_H(\vec{r})$ is the Hartree potential which is given by:

$$V_H(\vec{r}) = \int \frac{\rho(\vec{r}_1)\rho(\vec{r}_2)}{|\vec{r}_1 - \vec{r}_2|} d\vec{r}_1 d\vec{r}_2 \quad (2-22)$$

While V_{xc} is the exchange and correlation potentials, it is given by:

$$V_{xc} = V_c + V_x \quad (2-23)$$

$$V_{xc}(\vec{r}) = \frac{\partial E_{xc}[\rho(\vec{r})]}{\partial \rho(\vec{r})} \quad (2-24)$$

Thus, the Kohn-Sham equation can be written as:

$$H\psi_i(\vec{r}) = \left[\frac{-\hbar^2}{2m} \nabla^2 + V_{eff}(\vec{r}) \right] \psi_i(\vec{r}) = \varepsilon_i \psi_i(\vec{r}) \quad (2-25)$$

So far, there is no systematic method for overcoming energy exchange and correlation. However, DFT was not effective in quantum chemistry until the 1990s, when estimated ion methods were significantly developed to help model the exchange-correlation relationship. DFT is now a leading tool for measuring electronic structure in a variety of fields [60].

2.6 The Exchange Correlation Functionals

There are various suggested forms for exchange and correlation energy in the literature. The Local Density Approximation (LDA), which depends only on density and is thus a local functional, was the first successful and straightforward form. The next step was the Generalized Gradient Approximation (GGA), which included the density derivative and information about the neighborhood, making it semi-local. In density functional theory, the two most widely used approximations to the exchange and correlation energies are LDA and GGA. Aside from LDA and GGA, there are many other functionalities [61].

2.6.1 Local Density Approximation (LDA)

Because the exact shape of the exchange-correlation energy is unknown, approximations have been created. The most common of which is the local-density approximation (LDA), which is written as an integral of a local function of the density with a value at each point in space equal to that of a homogeneous electron gas. Despite its seeming crudeness, this approximation has been successful in a variety of systems, including those with quickly changing densities. However, although numerous approaches have been devised, it is not easy to enhance the LDA systematically when qualitative and quantitative differences between experiment and theory in solids arise [62].

2.6.2 Generalized Gradient Approximation (GGA)

The generalized gradient approximation (GGA) improves on the LDA by introducing gradient terms to account for density change near r . In contrast to the LDA, the GGA formulation does not have a single definition, and there are diverse kinds.

In a similar way to the LDA, the GGA is extended to magnetically polarized systems. The GGA works in some regions where the LDA fails, but it is not a

universally superior solution to the local approximation. The GGA is based on the undervaluation of the exchange energy and enhancement of the correlation energy in the LDA. However, the opposite nature of these corrections results in inconsistent improvements as different materials are treated. Before deciding between the LDA and GGA, cautious testing and comparison to measured values for a given material are required [63]. The GGA improves this description by considering the gradient of the electron density at the evaluation point. For most chemical issues, such techniques are crude, but they scale effectively for more extensive systems; meta-GGA functionals retain the convenient scaling qualities while also improving accuracy by introducing a dependency on the kinetic energy density [64].

2.7 Hybrid Functionals

Hybrid functionals are an approximation to the exchange-correlation energy functional in density functional theory (DFT). It combines a portion of Hartree-Fock theory's exact exchange with exchange and correlation from other sources like ab initio or empirical methods. The precise exchange energy functional is called an implicit density functional since it is described in terms of the Kohn-Sham orbitals rather than the density. A hybrid exchange-correlation functional is typically built on a linear combination of the Hartree-Fock exact exchange functional (E_x^{HF}) and correlation density functionals (E_c^{DFT}) [65].

The Hybrid function B3LYP represents (Becke, three-parameter, Lee-Yang-Parr) exchange-correlation functional [66]:

$$E_{xc}^{B3LYP} = E_{xc}^{LDA} + a_0(E_x^{HF} - E_x^{LDA}) + a_x(E_x^{GGA} - E_x^{LDA}) + a_c(E_c^{GGA} - E_c^{LDA}) \quad (2-26)$$

a_0 , a_x , and a_c are three empirical parameters, and the value of these parameters had been found as follow [$a_0 = 0.20$, $a_x = 0.72$, and $a_c = 0.81$] [65].

2.7.1 Coulomb-Attenuating Method (CAM B3LYP)

The CAM-B3LYP functional is a new hybrid exchange-correlation functional. It combines the hybrid properties of B3LYP with a long-range correction proposed by Tawada and coworkers. It was shown that CAM-B3LYP produces atomization energies that are equivalent to those produced by B3LYP [67]. Then it was shown that it could accurately explain charge-transfer transitions in big aromatic compounds, something that traditional LDA, GGA, and hybrid functionals could not do [68].

In a short, CAM-B3LYP combines the advantages of hybrid functionals like B3LYP with the advantages of long-range corrected functionals. The exchange functional is a mix of exact (Hartree–Fock) and DFT exchange, although unlike B3LYP, the ratio of exact to DFT exchange varies over the molecule [69].

2.8 Basis Sets

A basis set is a collection of mathematical functions used to construct the quantum mechanical wavefunction for a system [70]. These functions are often centered on atomic nuclei, with numerous basis functions representing the electron distribution surrounding each atom; integrating atomic basis functions produces the electron distribution in the entire molecule. A particular type of basis function known as a Slater-type orbital (STO) is a good approximation to atomic orbital wavefunctions. But is difficult to evaluate; therefore, most basis sets use various combinations of Gaussian-type orbitals (GTOs) to approximate the STOs. Only the minimum number of basis functions is sufficient to describe all of the electrons on each atom in a minimal basis set [64].

2.8.1 Slater Type Orbitals (STO's)

STO was developed by Zener and Slater for multi-electron atoms [71, 72]. The functional form of Slater type orbitals is [73]:

$$X^{STO} = Nr^{n-1}e^{\xi r}Y_{LM}(\theta, \phi) \quad (2-27a)$$

Where n , is a principal quantum number, the spherical harmonic functions Y_{LM} are the conventional spherical harmonic functions, N is a normalization constant, and ξ is the orbital exponent and given by:

$$\xi = \frac{z-S}{n^*} \quad (2-27b)$$

Where z is the number of atoms, S is a protection parameter, n^* is active principal quantum number.

The exact decay behavior of the orbitals for the hydrogen atom is mirrored by the exponential dependency on the distance between the nucleus and the electron. Due to the lack of radial nodes in STOs, nodes in the radial part are created by forming linear combinations of STOs. Although the exponential dependence assures a fairly fast convergence as the number of functions increases, analytical calculation of three- and four-center two-electron integrals is impossible. STOs are generally utilized in atomic and diatomic systems where great accuracy is required, as well as in semi-empirical approaches that ignore all three and four center integrals [30].

2.8.2 Gaussian Type Orbitals (GTO's)

In today's atomic and molecular calculations, Gaussian orbitals are widely used. The easiest integral polycentric functions are the most advantageous type of these functions. The general form of (GTOs) and (STOs) are the same, but the exponents differ. The Gaussian type orbital can be given by the following equation [74]:

$$\Phi_{nlm}^{GTO}(r, \theta, \phi) = R_{nl}(r)Y_{lm}(\theta, \Phi) \quad (2-28)$$

$$\text{Where } R_{nl}(r) = N_n r^{n-1} \exp(-\xi r^2) \quad (2-29)$$

Where N , is a normalization factor. The r^2 dependence in the exponential is a deficiency of the GTOs with respect to the Slater-type orbitals STOs.

The radial type in Gaussian type orbitals (GTOs) is determined by $\exp(-\zeta r^2)$ rather than $\exp(\xi r)$. The electron-electron repulsion integrals may now be computed analytically, whereas they can only be done numerically with STOs. The advantage of Gaussian type orbitals is that the central four – electron integrals that appear in self – consistent fields can be reduced to central two – electron integrals [75].

2.9.1 Minimal Basis Sets

The minimal basis set is made up of the minimum number atomic orbitals that are required to hold all of the electrons in a specific atom. The use of a minimum basis set for molecular systems has two drawbacks. One flaw is that all basis functions are either spherical, like s function, or occur in groups that describe a sphere, like p functions. As a result, molecules entirely made up of atoms in a spherical environment are better represented by a minimal basis set than molecules wholly composed of atoms in an aspherical environment.

The other flaw of minimal basis sets is that the basis functions are atom centered. This limits the flexibility of the functions used to represent the distribution of electrons between nuclei in chemical bonds. As a result of these flaws, molecules become overly ionic, and bonds become too long. The obvious solution to both shortcomings is to expand the basis set with more functions. An expanded basis set means more adjustable parameters in the variational optimization; however, this comes at the cost of increased computational effort [76].

Minimal basis sets are the smallest basis sets. The STO-3G set is the most widely used minimum base set. This notation implies that the basis set uses a single contraction of three GTO orbitals to approximate the shape of an STO orbital. Each orbital would then be given its contraction, which is the concept of a

minimum basis. For massive molecules, qualitative outcomes, and in some cases quantitative results, minimal basis sets are used. There are STO-nG basis sets when $n = 2-6$ [40].

2.9.2 Split-Valence Basis Sets

Pople's group [59], recently succeeded in preparing a small split-valence basis 3-21G, likely as a result of the success of the 4-21G basis set created by Pulay [60], using the computer program TEXAS and the gradient approach [61]. They initially determined 6-21G basis sets to prevent the collapse of the 3-21G valence component to avoid undesirable failure of the valence part of 3-21G. The 6G inner-shell functions were changed by smaller 3G inner-shell functions without reoptimizing the valence functions [77] .

2.9.3 Polarized Basis Sets

One or two asterisks, such as 6-31G* or 6-31G**, can be added to the Pople basis set notation. A single asterisk denotes adding a set of d primitives to atoms other than hydrogen. A set of p primitives has also been added to hydrogen, as shown by two asterisks. These are known as polarization functions because they allow the wave function to change shape more quickly. Adding polarization functions reduces variational total energy by roughly the same amount as adding another contraction. But, because this energy change is almost entirely systematic, it has a minor impact on relative energies. Because polarization functions often result in more exact calculated geometries and vibrational frequencies, they are frequently used [40].

2.9.4 Diffuse Basis Sets

Theoretical studies of negatively charged species have been discouraged due to the difficulties connected with ab initio calculations for anions. While standard split-valence basis sets reproduce anions the experimental geometries satisfactorily, energy assessments are problematic even when polarization basis sets and electron correlation adjustments are used. Although it has long been recognized that adding an extra set of diffuse functions to the basis set can significantly enhance anions results, no systematic examination of very small basis sets increased with diffuse functions has been conducted until now [78]. When using the spread function, it is commonly shown by the symbols below.

+ For heavy atoms except hydrogen.

++ For heavy atoms and hydrogen.

For instance, a valence split function for heavy atoms is 6-31+G.

6-31++G is a heavy atom and hydrogen valence split function.

2.10 Electronic Properties

2.10.1 HOMO, LUMO, and Energy Gap

The highest occupied molecular orbital (HOMO) and the lowest unoccupied molecular orbital (LUMO) are the two most important molecular orbitals. These orbitals are called the frontier orbitals as they lie at the outmost boundaries of the electrons of the molecules. The (HOMO), which is the highest energy (outermost) orbital containing electrons, is the orbital acting as an electron donor. The highest occupied molecular orbital (HOMO) and the lowest unoccupied molecular orbital (LUMO) is the most important in Molecular Orbitals Theory. On the other hand, the (LUMO), is the Lowest energy (innermost) orbital having space to accept electrons. The band gap regards the difference of the energies between the (HOMO) and (LUMO) Levels ($E_{gap} = E_{LUMO} - E_{HOMO}$) HOMO and LUMO and their resulting energy gap not only determine the way the molecule interacts with other species, but their energy gap (frontier orbital gap) helps characterize the chemical reactivity and kinetic stability of the molecule. A molecule with a small frontier orbital gap is more polarizable and is generally associated with a high chemical reactivity, Low kinetic stability and is also termed as soft molecule. The representation of (HOMO), (LUMO) energy Level and band gap for the interaction of two different molecules is shown in Figure 2.2, clearly Figure 2.3 shows an electron transfer to a higher energy state filling unoccupied molecular orbitals, and is call the excited state from the ground state [41].

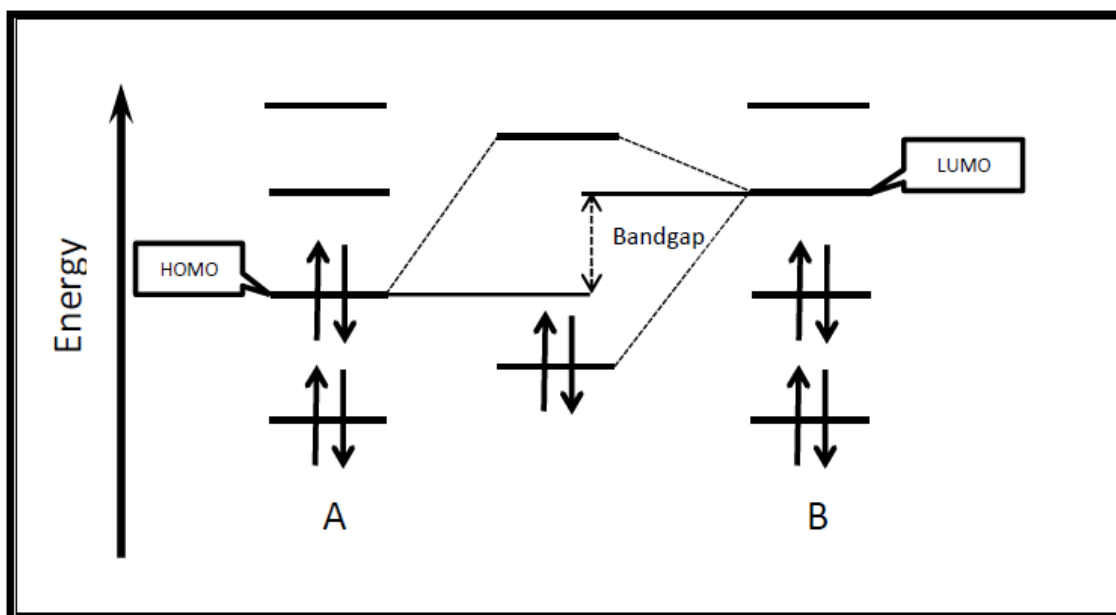


Fig 2.2: HOMO- LUMO and band gap diagram with two interacting molecules [79].

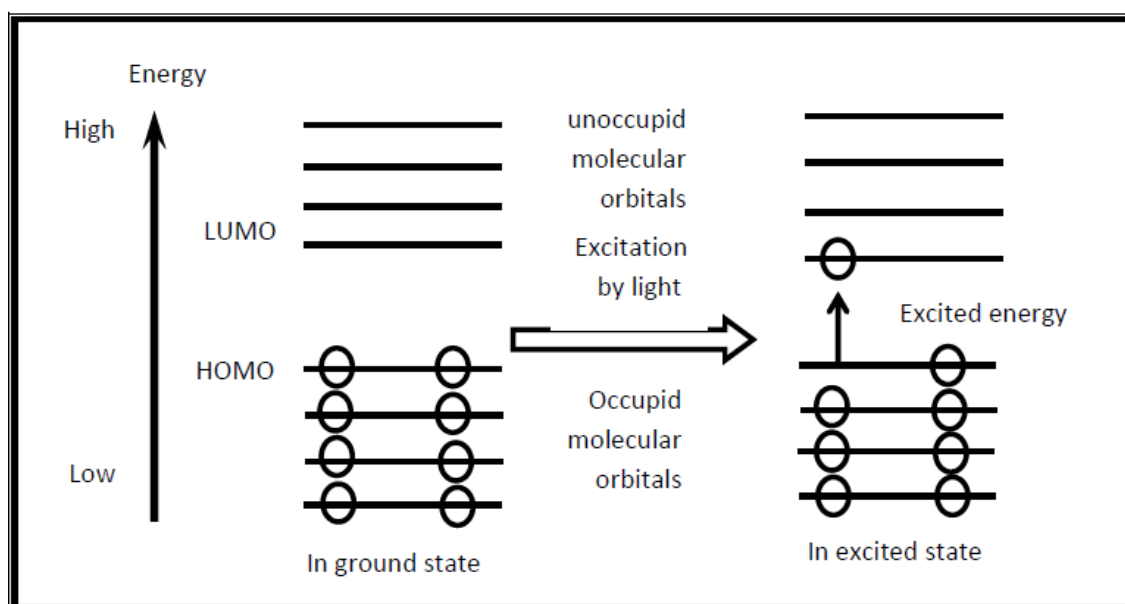


Fig 2.3: HOMO- LUMO diagram in ground and excited state [79].

2.10.2 Ionization Potential (I)

Ionization potential and electron affinity are relating directly to two interacting molecular orbitals, HOMO, the highest occupied molecular orbital and LUMO, the lowest unoccupied molecular orbital [80].

Ionization potential is defined as the capability of the molecule or ion to give electrons to the acceptors or simply the energy needed to detach the electrons from the system. According to Koopman's approach, HOMO energy (ϵ_H) is related to the ionization potential, as in the equation below [81, 82]:

$$I = -E_{HOMO} \quad (2-30)$$

Where E_{HOMO} : is the highest occupied orbital (one electron eigen value energy according to Khon-Sham DFT). A low value of ionization potential indicates a better electron donor molecule. It depends on the amount of the HF exchange term that included in the exchange-correlation functional [83].

2.10.3 Electron Affinity (A)

Electron affinity is known as the capability of the molecule or ion to gain the electrons from the donors or the energy shift that occurs when electrons collect on a neutral atom to form a negative ion [84]. LUMO energy (ϵ_L) is related to the electron affinity and given by [81]:

$$A = -E_{LUMO} \quad (2-31)$$

Where E_{LUMO} is the lowest unoccupied orbital. A high electron affinity reflects the better electron acceptor molecule.

2.10.4 Hardness (η)

The hardness of an atom, ion, or molecule known as a qualitative measure of how polarizable it is, or how much an electric field deforms its electron cloud. The

hardness of the interacting molecules is related to their stability. It can be evaluated using the following mathematical representation [85, 86]:

$$\eta = \frac{(I-A)}{2} \quad (2-32)$$

2.10.5 Softness (s)

Softness is a metric that measures the degree of the charge transfer inside a molecule. The small HOMO-LUMO energy gap of the molecules makes it soft and require very little energy to excite. In respect of reactivity, molecules with a high softness value are more reactive and less stable than hard molecules. Simply, the reciprocal of the hardness is the softness [85, 87]:

$$S = \frac{1}{\eta} \quad (2-33)$$

2.10.6 Electronegativity (χ)

Electronegativity refers to the ability of a molecule to attract electrons to itself. According to Mulliken, it can be achieved by the negative average value of the HOMO and LUMO energy as follow [85, 87]:

$$\chi = \frac{(I+A)}{2} \quad (2-34)$$

2.10.7 Electrophilicity Index (ω)

Electrophilicity index (ω) measures the energy reduction of a molecule due to electron stream between the donor and the acceptor[88]. It can be calculated from the following mathematical expression [89].

$$\omega = \frac{\rho^2}{2\eta} \quad (2-35)$$

The high electrophilicity index value reflects the better electron acceptor properties.

2.10.8 Chemical Potential (ρ)

Parr and his coworkers explained how the chemical potential links the DFT with the theories of structural chemistry. The chemical potential that appears in the DFT equation was identified with the negative of the electronegativity. The quantity in equation (2-36) often used to explain charge transfer during the process of molecular formation, is a sort of energy that may be released or absorbed based on the number of electrons in the molecule [90, 91].

$$\rho = \frac{-(I+A)}{2} \quad (3-36)$$

2.10.9 Polarizability and First Order Hyperpolarizability

The dipole moment (μ), polarizability (α), and first order hyperpolarizability (β) of the DAP molecule are studied based on finite-field technique to find the link between molecular structure and non-linear optic characteristics (NLO) [92]. The tensors can be determined using frequency job of Gaussian Program. Instead of atomic units (a.u.), it is more convenient to convert the tensor units generated from the output file to electrostatic units (esu).

The total dipole moment can be evaluated in term its components using the equation [92]:

$$\mu_{tot} = (\mu_x^2 + \mu_y^2 + \mu_z^2)^{1/2} \quad (2-37)$$

The mean polarizability $\bar{\alpha}$ and the anisotropy of the polarizability ($\Delta\alpha$) can be calculated using the following equations [93]:

$$\bar{\alpha} = \frac{1}{3}(a_{xx} + a_{yy} + a_{zz}) \quad (2-38)$$

$$\Delta\alpha = \frac{1}{\sqrt{2}} \left[(\alpha_{xx} - \alpha_{yy})^2 + (\alpha_{yy} - \alpha_{zz})^2 + (\alpha_{zz} - \alpha_{xx})^2 + 6\alpha_{xz}^2 + 6\alpha_{xy}^2 + 6\alpha_{yz}^2 \right]^{1/2} \quad (2-39)$$

The average value of the first hyperpolarizability $\langle\beta\rangle$ can be given by [16]:

$$\langle \beta \rangle = \left[(\beta_{xxx} + \beta_{xyy} + \beta_{xzz})^2 + (\beta_{yyy} + \beta_{yzz} + \beta_{yxx})^2 + (\beta_{zzz} + \beta_{zxx} + \beta_{zyy})^2 \right]^{\frac{1}{2}} \quad (2-40)$$

2.11 Vibrational analysis

2.11.1 Infrared Spectroscopy

Infra means under, in the infrared region, and the frequency of infrared less than the red rays in the visible electromagnetic spectrum. Devices that use infrared rays can see in complete darkness because they depend on the heat radiation emitted by the objects. The infrared spectrum lies between the visible spectrum and the microwave spectrum. It covers a wide area of the electromagnetic spectrum.

Infrared radiation absorbed organic and inorganic molecules and convert it into stretching, vibrational and bending molecular energy, infrared radiation is lowest in energy than visible radiation. The electromagnetic spectrum of the infrared region is divided into three parts [94]. The near-infrared region lies between 13000-4000) cm^{-1} mid region between (4000-200) cm^{-1} and far region (200-10) cm^{-1} .

The N-atoms system absorbs amount of energy will oscillate with three degrees of freedom for both translation and rotation, and (3N-6) degrees of freedom for vibration for ring molecules. The vibration analysis is valid only when the first derivative of the energy with respect to displacement of the atoms is zero. Also, the analysis at transition states and higher order saddle point is valid [95].

The number of vibrational transitions in a molecule depends on the number of its constituent atoms, as well as on the spatial distribution of the molecule, i.e. whether the molecule is linear or non-linear.

-The number of vibrational modes in the case of linear molecules is 3N-5.

- The number of vibrational modes in the case of nonlinear molecules is $3N-6$.

Where, N is the number of atoms in the molecule. And this represents the modes of vibration.

2.11.2 Raman Spectroscopy

Raman effect depends upon the polarizability of the molecule, it can be observed for molecules which have no net dipole moment and therefore produce no pure rotational spectrum. This process can yield information about the moment of inertia and hence the structure of the molecule. Light scattering by molecules or crystal lattices has a negligible effect. When monochromatic light is scattered by molecules or crystal lattices, spectral analysis reveals a strong spectral line that matches the light source's wavelength. Additionally, weaker lines are visible at wavelengths that are displaced from the light source's wavelength. Raman lines are the name for these lines (after the Indian physicist Chandrasekhara Venkata Raman). Despite the fact that these lines had been theoretically predicted, Raman was the first to actually prove them in 1928 [96] .

2.12 Computer used

1. Laptop DELL
2. System: Windows 10 - 64-bit
3. Hard disk: 500 GB
4. RAM: 4.00 GB
5. Intel Core i3-4005U CPU @ 1.70GHz 1.70 GHz

Chapter Three

Results and Discussion



CHAPTER THREE

RESULTS AND DISCUSSION

3.1 Introduction

The results obtained using the DFT method with hybrid function CAM B3LYP and HF method have been explained and discussed in this chapter. It consists of three main parts; the first is represented by the conformational properties such as the potential energy surface, the lowest energy to get the optimization structure, the bond lengths, bond angles, and dihedral angles. The electronic properties were the second part; they have included charge distribution, dipole moment, Polarizability and first-order hyper-polarizability, and the energies of seven global parameters. The last part is devoted to vibrational spectroscopy like Infrared spectroscopy and Raman Spectroscopy. All calculations have been performed using Gaussian 09 [97], and visualized by Gauss View 06 [98].

3.2 Building the Monomer of DAP

The monomer DAP as shown in Figure 3.1 consists of 14 atoms of carbon, 14 atoms of hydrogen and 4 atoms of oxygen. It has been built using the Gauss View 6 software program and optimized using Gaussian 09 program to obtain its structural and electronic properties. The density functional theory DFT and hybrid function CAM B3LYP with basis set 6-311+G (d, p) were used to calculate these properties.

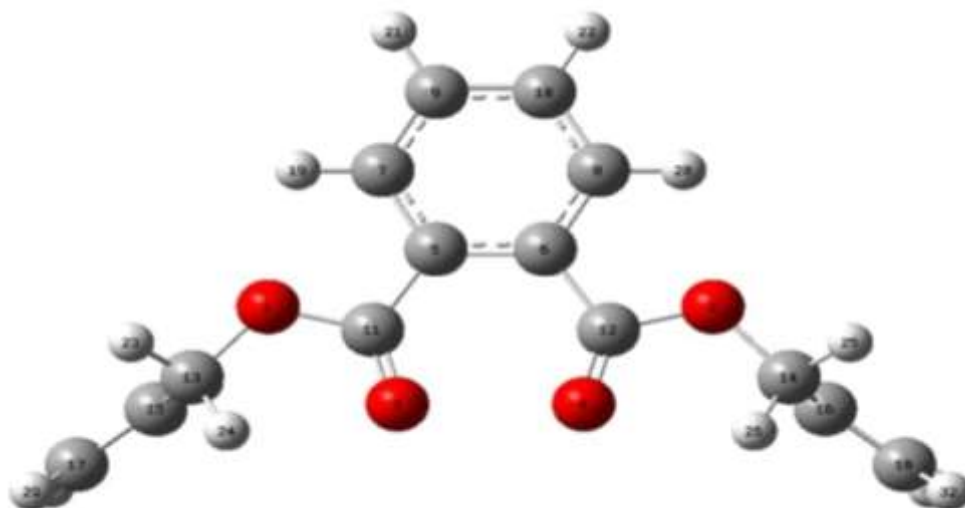
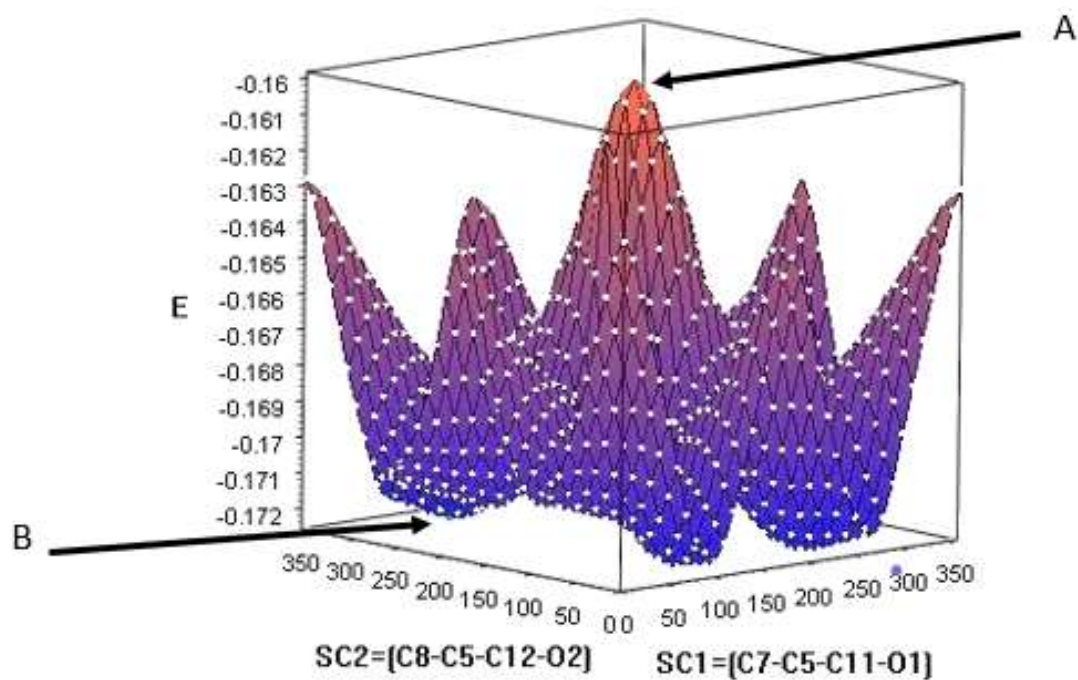


Fig. 3.1: The DAP monomer drawing by Gauss View 06 program.

3.3 Potential Energy Surface Scan (PES) of DAP

After the building of the monomer, the Potential Energy Surface (PES) scan has been used to determine the partial optimization of the monomer. A potential energy surface is a graphical or mathematical relationship between the energy of a molecule and its geometry. The scan has been performed for the dihedral angles $SC_1 = C_7-C_5-C_{11}-O_1$ and $SC_2 = C_8-C_6-C_{12}-O_2$, see Figure 3.1, using Semi-empirical method PM6. In this process, the dihedral angles SC_1 and SC_2 are changed from 0° - 360° by 10° for each step. While the dihedral angles are changed through the scan calculations, all the other geometries are left to be relaxed. After that, the scan grid is produced consisting of 1369 molecules with different energies and many global maximum and minimum as shown in Figure 3.2. To find the most stable molecule among the 1369 molecules, the lowest energy molecule should be found. Therefore, molecule 477 which has the $SC_1 = 120^\circ$ and $SC_2 = 320^\circ$, is considered the stable one with minimum energy equal to (-0.172583) Hartree.



B Molecule 477

A Molecule 685

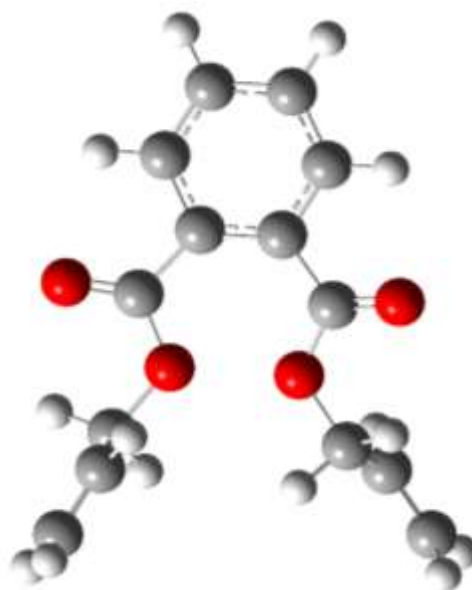
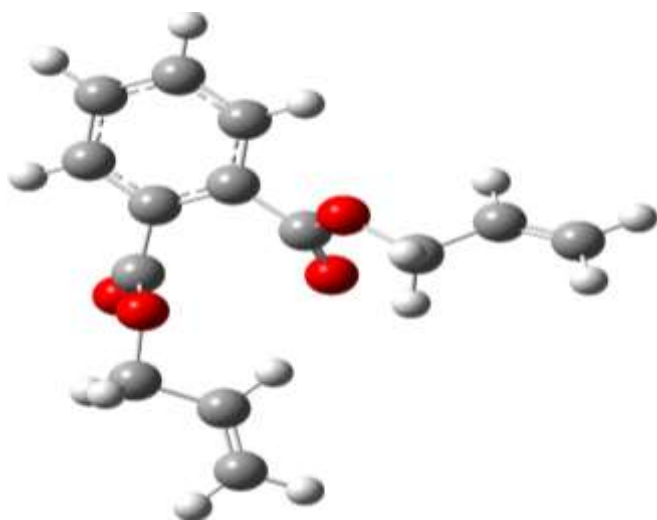


Fig. 3.2: Shows (A) Molecule 685 with $SC_1=180^\circ$, $SC_2=180^\circ$, and $E = -0.159834$ Hartree (maximum energy). (B) Molecule 477 with $SC_1 = 120^\circ$, $SC_2 = 320^\circ$ and $E = -0.172583$ Hartree (minimum energy).

3.4 Full Optimization of the DAP

After the potential energy surface, the DAP monomer 477 is fully optimized by using the DFT-CAM B3LYP with 6-311+G (d, p) basis set and without symmetry restrictions. The resulting molecule was found to be converged to optimized geometries with minimum energy equal to -842.614348 Hartree. The use of the DFT led to slight changes into the dihedral angles SC_1 and SC_2 from 120° and 320° to 123.44° and -30.23 or (329.77°) . The potential energy curve has been used to ensure that the dihedral angles using DFT are accurate. To generate the energy curve, the dihedral angles SC_1 and SC_2 are changed from 20° to 160° and -120° to 0° , respectively. Figure 3.3 shows that the total electronic energy decreases with the dihedral angles until about 123° ; it changes its behavior to increase with the increasing dihedral angles. Figure 3.4 behavior the same with the lowest energy lies at 229.77° . These results confirm that the dihedral angles that lead to the molecule's energy are accurate.

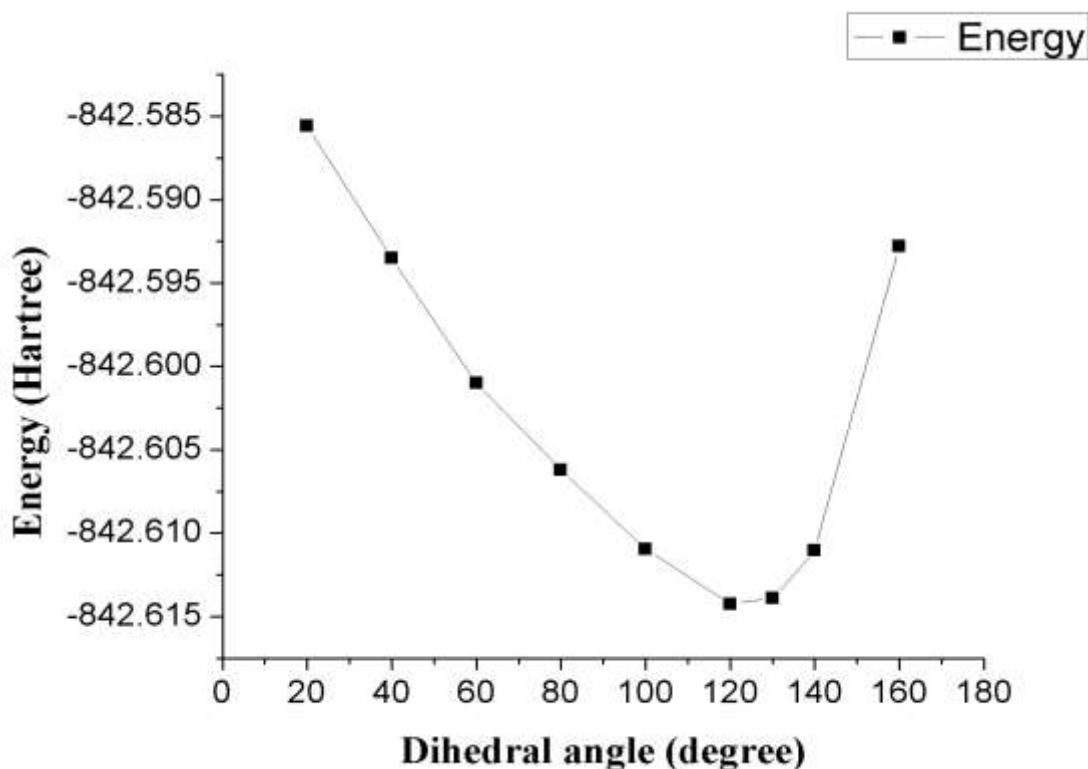


Fig. 3.3: The potential energy curve for the angle SC_1 ($C_7-C_5-C_{11}-O_1$).

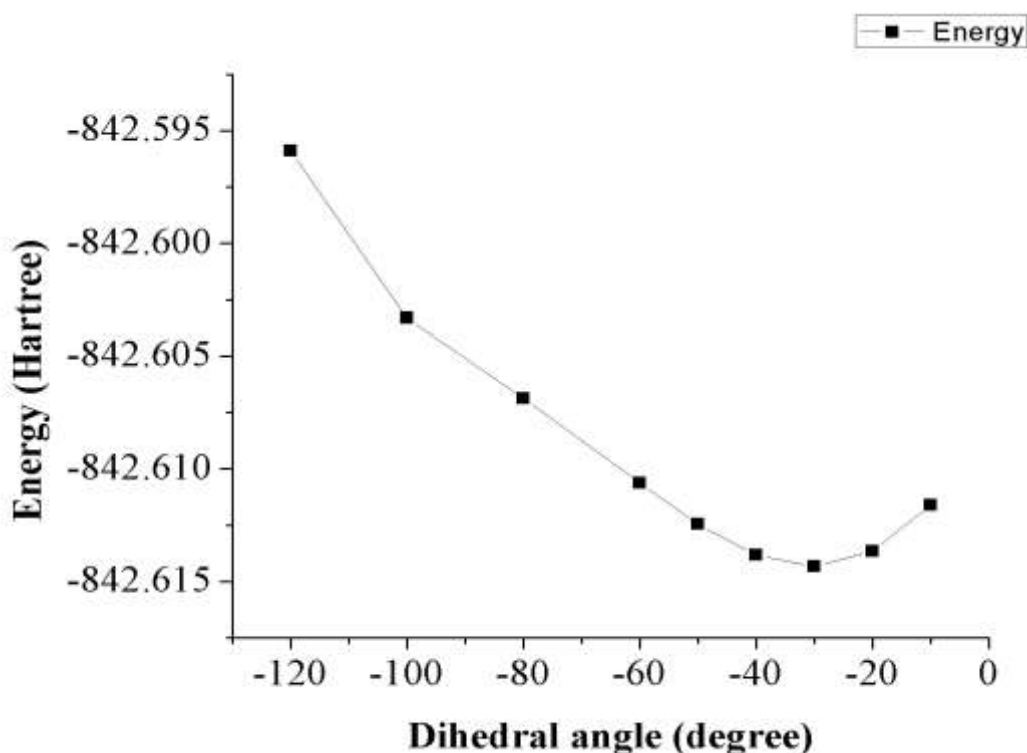


Fig 3.4: The potential energy curve for the angle SC_2 ($C_8-C_6-C_{12}-O_2$).

It is worth noting that molecule 477 has been optimized using the Hartree-Fock method. The total electronic energy evaluated by this method is equal to -837.953983 Hartree. This energy value indicates that the HF method gives a less stable molecule than the CAM-B3LYP method. The aim of using the HF method is to compare and show the difference in the results.

3.5 Structural Properties

3.5.1 Bond Lengths

It is likely fair to state that bond lengths have been used more than any other molecular parameter for determining the type of chemical bonds. Even with relatively rudimentary bond length measurements, some of the gross impacts of the molecular environment on the bond between two atoms have been detected.

As molecular structure theories have been developed, there has been a trend to attribute significance to smaller and smaller differences in measured bond lengths. While experimental procedures have advanced simultaneously, there has not always been a one-to-one correspondence [99].

For a small number of molecules, several relationships between force constants or vibrational frequencies and bond distances have been discovered to hold approximately. They usually have two or more variables that depend on the atoms that constitute the bond or their location in the periodic table [100].

For this work, the results conducted for the DAP using both the DFT and HF methods are shown in Figure 3.5 and listed in Table 3.1. Because there is no experimental or calculated data for the diallyl phthalate, the results of this work have been compared with those of the dimethyl phthalate ion [19]. The results show that the bond lengths calculated using the DFT-CAM B3LYP with the basis set of 6-311+G (d, p) are better than those found using the HF at the same basis set. The average values of the bond lengths of the carbon atoms for the benzene ring are 1.389 and 1.386 in Angstrom units (Å) for DFT and HF methods, respectively. In comparison, it was 1.403 Å for calculated data by Gerbaux [19]. For the aromatic hydrogen atoms, the average values of the bond are 1.082 and 1.074 Å for both methods, respectively. In addition, the average values of the bond lengths of the diallyl (C and O atoms) are 1.383 and 1.374 Å for both methods, respectively.

For comparison purpose, the average values of diallyl (C and O atoms) for the range C₅-C₁₃ and C₆-C₁₄ are found to be 1.370 and 1.357 Å compared to calculated value which is 1.371 Å. The average values of hydrogen atoms for diallyl are found to be 1.086 and 1.078 Å for the both DFT and HF, respectively. It is worth mentioning here that the lengths of the single bond C-C atoms outside the ring (like C₅-C₁₁ and C₁₃-C₁₅) are larger than the aromatic bond lengths. This behavior occurs because the p-electrons and then the resonance of the benzene

ring. Each carbon atom contains one p-electron and these electrons are overlapping with each other to form a system of π -orbitals which spread out over the carbon atoms. The six electrons will be delocalized in three molecular orbitals because they are no longer held between just two carbon atoms. This delocalization gives the benzene ring more stability. As a result, there will be identical bond lengths between carbon atoms and less than those outside the ring.

It is also noticeable that the $C_{11}=O_3$ double bond shorter than the $C_{11}-O_1$ bond because it has a higher electron density and hence its electrons occupy more space than electrons of single bond (the force of attraction between atoms is more significant in the double bond, causing the atoms to be pulled). The same situation can be seen for the $C_{15}-C_{13}$ and $C_{15}=C_{17}$ bonds. The high electronegativity of oxygen atoms brings the electron density toward the nucleus and this makes the bond lengths of the $C_{13}-O_1$ shorter than those of the $C_{13}-C_{15}$, see Table 3.1.

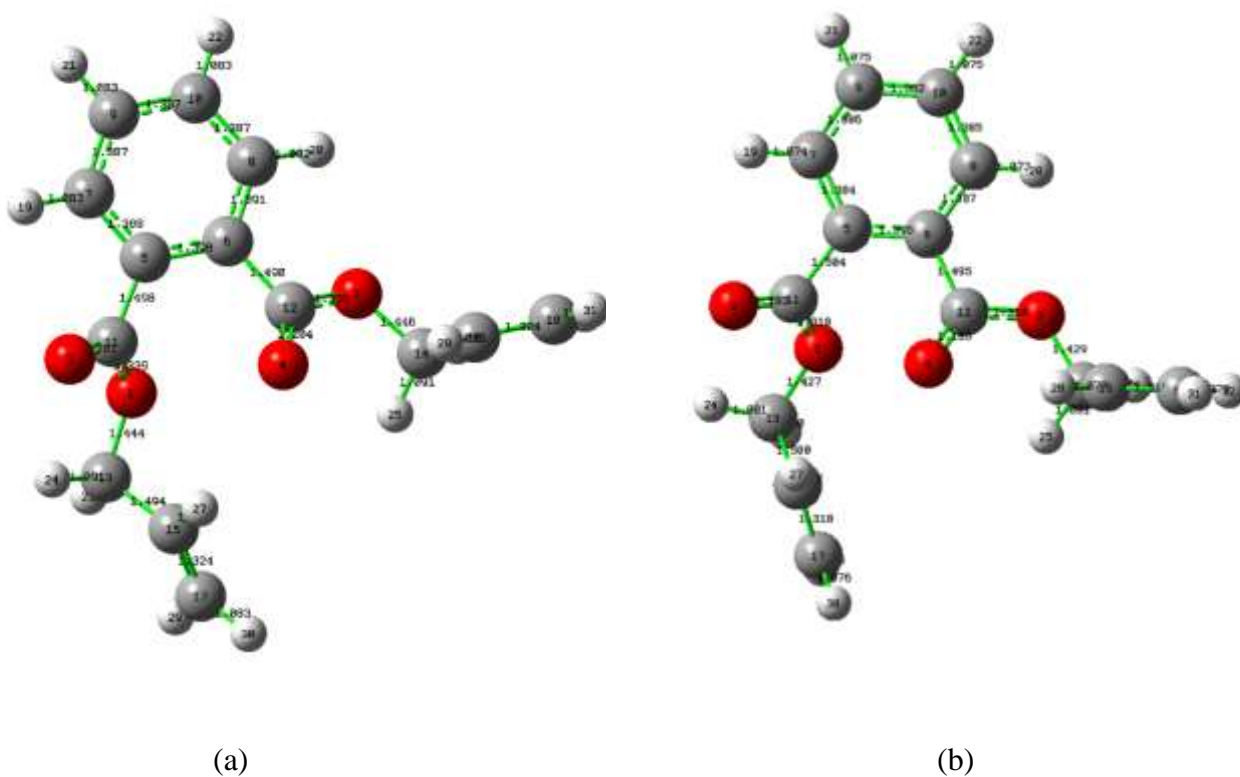


Fig 3.5: The bond lengths of diallyl phthalate using the (a) DFT and (b) HF method.

Table 3.1: The bond lengths (\AA) of the DAP using the DFT and HF methods.

Parameter	DFT	HF	Ref. [19]
$\text{O}_1 - \text{C}_{11}$	1.339	1.318	1.288
$\text{O}_1 - \text{C}_{13}$	1.444	1.428	1.480
$\text{O}_2 - \text{C}_{12}$	1.338	1.318	1.321
$\text{O}_2 - \text{C}_{14}$	1.446	1.429	1.458
$\text{O}_3 = \text{C}_{11}$	1.201	1.183	1.225
$\text{O}_4 = \text{C}_{12}$	1.204	1.186	1.211
$\text{C}_5 - \text{C}_6$	1.398	1.395	1.424
$\text{C}_5 - \text{C}_7$	1.388	1.384	1.421
$\text{C}_5 - \text{C}_{11}$	1.498	1.504	1.492
$\text{C}_6 - \text{C}_8$	1.392	1.387	1.380
$\text{C}_6 - \text{C}_{12}$	1.490	1.495	1.502
$\text{C}_7 - \text{C}_9$	1.387	1.386	1.379
$\text{C}_8 - \text{C}_{10}$	1.387	1.385	1.413
$\text{C}_9 - \text{C}_{10}$	1.387	1.382	1.405
$\text{C}_{13} - \text{C}_{15}$	1.494	1.500	1.540
$\text{C}_{14} - \text{C}_{16}$	1.495	1.500	1.540
$\text{C}_{15} = \text{C}_{17}$	1.324	1.318	1.340
$\text{C}_{16} = \text{C}_{18}$	1.324	1.319	1.340

To sum up, the bond lengths results which achieved using the DFT give a good agreement with the result calculated by Gerbaux as shown in Figure 3.6. This Figure shows a linear correlation between these results, with correlation factor (R^2), which is equal to 0.949 and 0.946 for the DFT and HF, respectively. These results give the preference to the DFT over the HF method. The following equations describe the bond length relationships:

$$d_{\text{cal.}} = 0.882d_{\text{theo.}} - 0.076 \quad (R^2 = 0.949) \quad \text{DFT method}$$

$$d_{\text{cal.}} = 0.949d_{\text{theo.}} - 0.055 \quad (R^2 = 0.946) \quad \text{HF method}$$

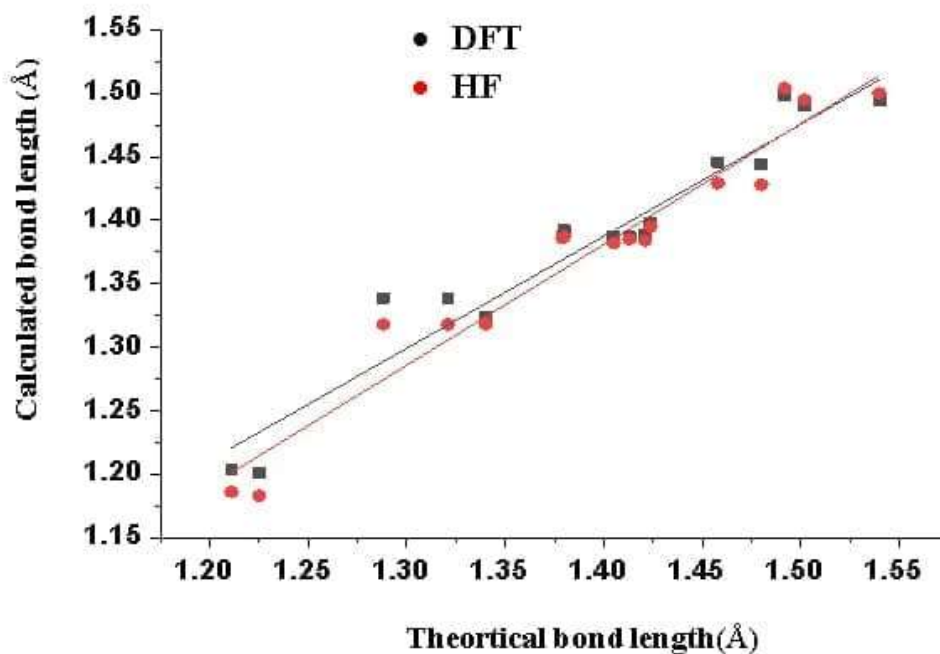


Fig 3.6: The linear correlation graph between of the theoretical bond lengths and those calculated in this work.

3.5.2 Bond Angles

A bond angle is an angle formed between three atoms across at least two bonds in the molecule or compound and it is measured in degree units. A molecule for only two atoms does not have a bond angle; at least three atoms are required for bond angles to appear. Bond angles and distances can be used to describe the geometry of a molecule or compound. The ideal bond angles are affected by many factors such as the presence of lone pairs, size of atoms that constitute a molecule, large groups connected to the central group, multiple bonds, as well as the environment in which the molecule is found.

The bond angles of the DAP are calculated by using CAM-B3LYP and HF methods with 6-311+G (d, p) in the gas phase. The obtained results are listed in Table 3.2.

Table 3.2: The bond angles (degree) of the DAP molecule using the DFT and HF methods.

Parameter	DFT	HF	R[15]
C₁₁-O₁-C₁₃	117.4	118.8	109.5
C₁₂-O₂-C₁₄	116.7	118.5	109.5
C₆-C₅-C₇	119.6	119.6	120.0
C₆-C₅-C₁₁	123.4	123.8	109.5
C₇-C₅-C₁₁	117.0	116.6	109.5
C₅-C₆-C₈	119.6	119.6	120.0
C₅-C₆-C₁₂	120.2	120.4	109.5
C₈-C₆-C₁₂	120.0	119.8	109.5
C₅-C₇-C₉	120.4	120.5	120.0
C₆-C₈-C₁₀	120.4	120.5	120.0
C₇-C₉-C₁₀	120.0	120.0	120.0
C₈-C₁₀-C₉	119.9	119.8	120.0
O₁-C₁₁-O₃	124.8	124.7	-
O₁-C₁₁-C₅	111.3	111.8	109.5
O₃-C₁₁-C₅	123.8	123.3	-
O₂-C₁₂-O₄	123.6	123.8	-
O₂-C₁₂-C₆	112.3	112.7	109.5
O₄-C₁₂-C₆	124.1	123.4	-
O₁-C₁₃-C₁₅	110.6	111.5	109.5
O₂-C₁₄-C₁₆	111.7	111.9	109.5
C₁₃-C₁₅-C₁₇	123.3	123.3	125.0
C₁₄-C₁₆-C₁₈	123.3	123.4	125.0

Table 3.2 shows that the angles of the benzene ring range from 119.6-120.4° with an average value is equal to 119.98° for the DFT method, whereas this range is found to be from 119.6-120.5° with a slightly different average to be 120° for the

HF method. The results of the aromatic angles show a fair agreement with the standard values, which is 120° for each angle, as shown in the Table 3.2. The similar values of the benzene ring angles are due to the similar environment of the atoms of that ring. In the diallyl chains, it is noticed that the angles $O_1-C_{11}-C_5$ and $O_2-C_{12}-C_6$ are short bond angles with values 111.3° and 112.3° . The lone pairs and double bonds of the oxygen atoms O_3 and O_4 are responsible for this behavior. The lone pairs of each oxygen atom mean that this atom has a higher electron density than the carbon atom. This density will be enhanced by the electron density produced by the double bond (remember the high electronegativity of the oxygen atom). The result is a solid repulsive force toward the bonds below the oxygen atoms O_3 and O_4 . Hence, the angles $O_1-C_{11}-C_5$ and $O_2-C_{12}-C_6$ will distort and get smaller.

3.5.3 Dihedral Angles

A dihedral angle or torsion angle is the angle between two planes. It can be defined by four atoms and visualized by looking down the central bond (i.e. the bond from atom 2 to atom 3). Only the distance between the first and fourth atoms affects the dihedral angle; the chemical bond lengths and angles control the other interatomic distances. Its degrees vary from -180 to $+180$. When a clockwise rotation is conducted with the molecule in its plane, the torsion angle is positive; when an anti-clockwise rotation is performed with the molecule in its plane, the torsion angle is negative. The Figure 3.7 shows the bond, angle, and dihedral angle.

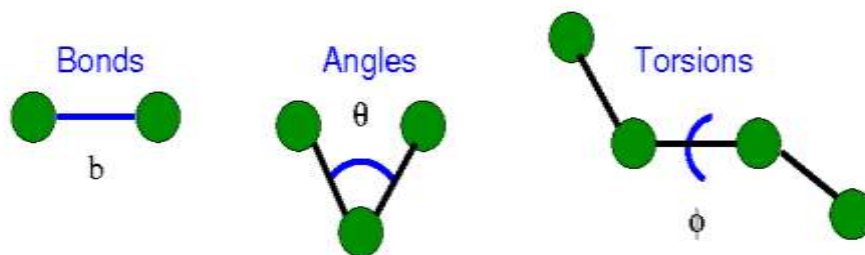


Fig. 3.7: The bond, angle, and dihedral angle diagram [101].

Table 3.3 reveals the dihedral angles of the diallyl phthalate molecule depending on the CAM-B3LYP and HF methods with the basis set 6-311+G (d, p). In general, all the hydrogen atoms in the benzene ring are sp^2 hybridized and hence they are trigonal planar with bond angles of 120° . The planarity of this ring makes all the dihedral angles are zero. For this work, all the dihedral angles of the benzene ring are very close to zero like the angle $C_7-C_5-C_6-C_8$ and $C_{11}-C_5-C_6-C_8$ with the values of 1.8 and 1.5 for the DFT and HF methods, respectively. The results of the benzene dihedral angles indicate that the connection of the two branches of carbon dioxide and allyl did not have any significant effect on the planarity of the ring. The largest values of dihedral angles can be found, for example, at $C_{13}-O_1-C_{11}-C_5$, $C_{11}-C_5-C_6-C_8$, and $C_{12}-C_6-C_8-C_{10}$ because the rigid connection of the atoms in benzene ring. The terminal dihedral angles $O_1-C_{13}-C_{15}-C_{17}$ and $O_2-C_{14}-C_{16}-C_{18}$ can rotate easily because of their terminal location and the single bond.

Table 3.3: The dihedral angles (degree) of the DAP using the DFT and HF methods.

Parameter	DFT	HF
C13-O1-C11-O3	-6.40	-4.20
C13-O1-C11-C5	178.3	-179.1
C11-O1-C13-C15	-96.1	-88.3
C14-O2-C12-O4	0.10	0.40
C14-O2-C12-C6	178.2	178.5
C12-O2-C14-C16	-81.4	-81.3
C7-C5-C6-C8	-1.80	-1.50
C7-C5-C6-C12	172.6	172.9
C11-C5-C6-C8	176.6	176.2
C11-C5-C6-C12	-9.00	-9.30
C6-C5-C7-C9	1.50	1.30
C11-C5-C7-C9	-176.9	-176.6
C6-C5-C11-O1	-55.0	-56.3
C6-C5-C11-O3	129.7	128.6
C7-C5-C11-O1	123.4	121.5
C7-C5-C11-O3	-51.9	-53.6
C5-C6-C8-C10	0.90	0.80
C12-C6-C8-C10	-173.6	-173.7
C5-C6-C12-O2	155.4	155.6
C5-C6-C12-O4	-26.6	-26.3
C8-C6-C12-O2	-30.2	-30.0
C8-C6-C12-O4	147.8	148.2
C5-C7-C9-C10	-0.30	-0.30
C6-C8-C10-C9	0.40	0.20
C7-C9-C10-C8	-0.70	-0.50
O1-C13-C15-C17	-126.1	-126.4
O2-C14-C16-C18	-118.1	-118.9

3.6 Electronic Properties

3.6.1 Natural Atomic Charge Distribution

Partially atomic charges are valuable descriptors for chemically intuitively comprehending the results of quantum chemical calculations. It simply refers to assigning a partial charge to each atom in a molecule to describe the electron charge distribution within it. Many different models have been developed to extract partial atomic charges from the molecular charge distribution since partial atomic charges are not physical observables and have no precise quantum mechanical description [102].

In this work, the charge distribution of the DAP according to the natural atomic charge distribution has been investigated at the CAM B3LYP and HF levels with a basis set of 6-311+G (d, p). The charges of each atom in the molecule are depicted in this calculation. The distribution of positive and negative charges is crucial in determining whether the bond length between the atoms increases or decreases. Figure 3.8 shows the charge distribution of the DAP molecule using a color range from red to green to represent the negative and positive charges.

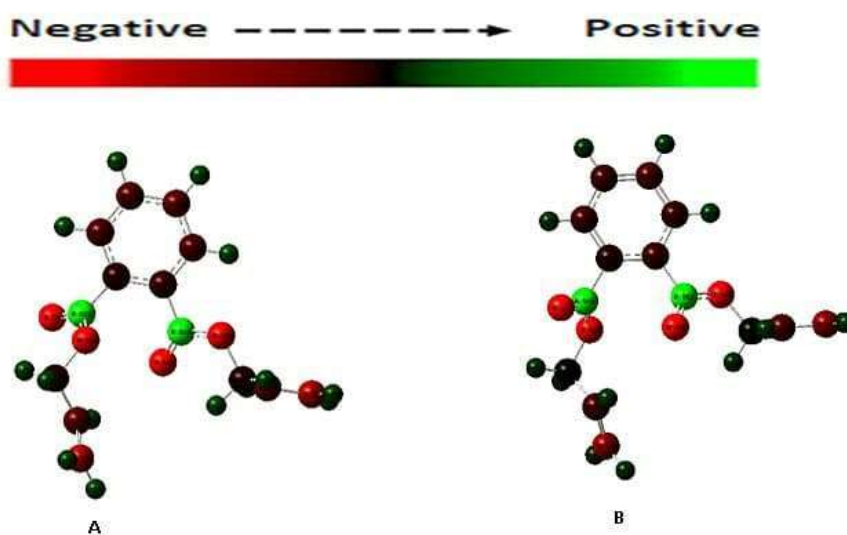


Fig 3.8: The natural atomic charge distribution for the DAP using (A) DFT (B) HF methods.

The calculated charges of the DAP molecule are given in Table 3.4 and plotted in Figure 3.9. From the Table 3.4, all the oxygen atoms (O_1 , O_2 , O_3 , O_4) have negative and similar values, which is expected because of the electronegativity of the oxygen [103]. The carbon atoms connected with hydrogen atoms (C_7 , C_8 , C_9 , and C_{10}) show negative charges with similar values. At the same time, C_5 and C_6 have slightly different values because of the substitute of the hydrogen atom by carbon. It is noticed that all the hydrogen atoms in the molecule are positive with similar values, which comes from hydrogen's ability to give its electron. The highest positive value is found in C_{11} and C_{12} connected to two oxygen atoms for each; the electronegativity of oxygen draws the electrons from the carbon atom and leaves it positive. The low negative values found in the carbon atoms C_{13} and C_{14} connected with two hydrogen atoms and one oxygen atom for each. Hydrogen atoms provide the carbon atoms with electrons while oxygen withdraws. The highest negative values of the carbon atoms are shown in C_{17} and C_{18} ; the reason is the two hydrogen atoms for each carbon and the absence of oxygen.

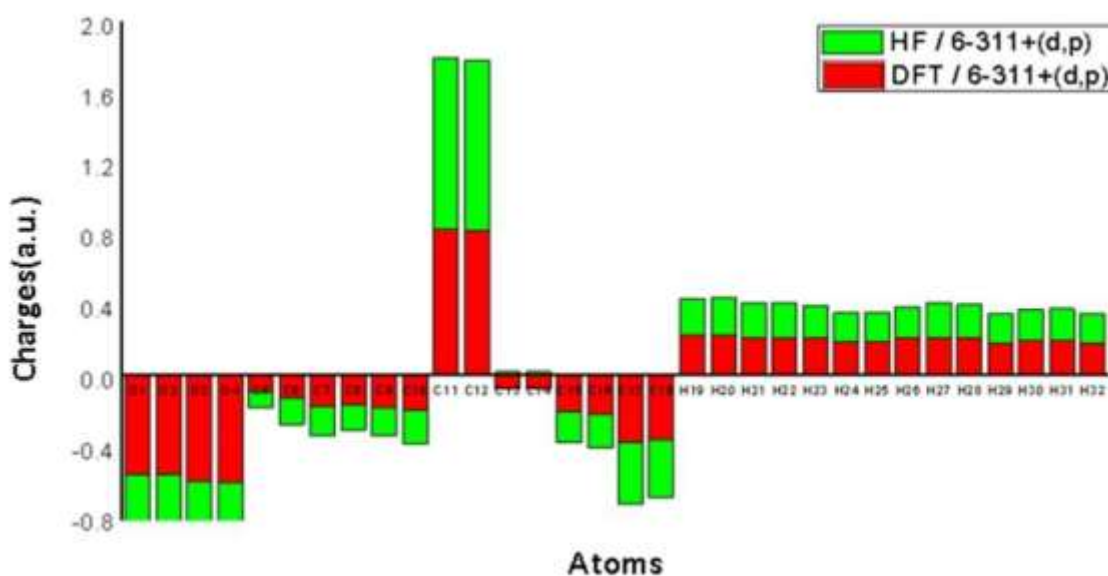


Fig 3.9: Natural atomic charge chart analysis at DFT and HF method of DAP molecular.

Table 3.4: The natural atomic charge of the DAP using the DFT and HF methods.

Atoms	Charges		Atoms	Charge	
	CAM B3LYP	HF		CAM B3LYP	HF
O₁	-0.55943	-0.63768	C₁₇	-0.37588	-0.34815
O₂	-0.55798	-0.63771	C₁₈	-0.35816	-0.32893
O₃	-0.59647	-0.67695	H₁₉	0.22730	0.21127
O₄	-0.60686	-0.68536	H₂₀	0.23053	0.21395
C₅	-0.08855	-0.08949	H₂₁	0.21485	0.19769
C₆	-0.12650	-0.14693	H₂₂	0.21455	0.19801
C₇	-0.17466	-0.16591	H₂₃	0.21587	0.18084
C₈	-0.16451	-0.13996	H₂₄	0.19261	0.16343
C₉	-0.18259	-0.15889	H₂₅	0.19550	0.16545
C₁₀	-0.19775	-0.18834	H₂₆	0.21152	0.18014
C₁₁	0.82873	0.96905	H₂₇	0.21818	0.19706
C₁₂	0.82432	0.96221	H₂₈	0.21160	0.19255
C₁₃	-0.07615	0.02190	H₂₉	0.18433	0.16640
C₁₄	-0.07330	0.02401	H₃₀	0.19699	0.17935
C₁₅	-0.19919	-0.17421	H₃₁	0.19830	0.18016
C₁₆	-0.21361	-0.19378	H₃₂	0.18643	0.16884

3.6.2 HOMO and LUMO

The HOMO-LUMO energies are popular quantum mechanical descriptors which play a major role in governing wide range of chemical interactions. When dealing with interacting molecular orbitals, the HOMO of one molecule and the LUMO of another molecule are usually the two orbitals that interact. Frontier orbitals, also known as HOMO and LUMO, are used to calculate the amount of energy required to add or remove electrons in a molecule. HOMO is a term that refers to the tendency of species to give an electron; it is expressed for nucleophilic components. In contrast, LUMO is related to the propensity to receive electrons

and is a feature of electrophilic components. The HOMO (highest occupied molecular orbital) and LUMO (lowest unoccupied molecular orbital) energies are involved in molecular orbital interaction [104]. The chemical reactivity, kinetic stability, chemical hardness, chemical softness, and optical polarizability of a molecule are all determined by the energy gap between HOMO and LUMO. The soft molecule is more polarizable than the hard one because it needs small energy to excitation.

In this work, 478 MOs were obtained, the first 65 MOs are completely filled with electrons, they called occupied MOs, and the remaining 413 MOs are empty and called unoccupied MOs. The energy level alignment of these orbits indicates that the 65th MO is the highest energy orbital among the occupied MOs and the 66th MO is the lowest energy orbital among the unoccupied ones. Figure 3.10 and 3.11 show the HOMO and LUMO for the DAP using the DFT and HF methods at the 6-311+G (d, p) basis sets. The positive phase is represented in green colour and the negative phase is represented in red colour. The Figures reveal that the HOMO more localized on the whole molecule than the LUMO. The latter is especially localized on phthalate part (benzene ring connected to two branches of carbon dioxide). The HOMOs are bonding type orbitals, π orbitals, with no electron density on the bonding axis, the bonding electron density lies above and below, or in front and in back of the bonding axis. In contrast, the LUMOs are anti-bonding type orbital, π^* orbital, with node between atoms. This node leads to zero electron density by which a repulsion between the two interacting atoms will be produced. Figures show that each sp^2 carbon is hybridized and the s-bond system is treated independently of the p-bonded system. This assumption is justified that the sp^2 -hybridized orbitals are orthogonal to the p-orbital on each carbon, and the electrons in the bonded s-orbitals are much lower in energy than those in the p-bonded system. Overlapping face-to-face orbitals provides a greater nuclear attraction to electrons than side-to-side interference.

The evaluated energy values of the HOMOs and LUMOs for the DFT and HF methods are listed in Table 3.5. The difference of energy between LUMO and HOMO is called energy gap, it is indicate the chemical stability of structures [105]. The table shows that the energy gap between the HOMO and LUMO is 8.326 eV for DFT while its value is 4.522eV for HF method.

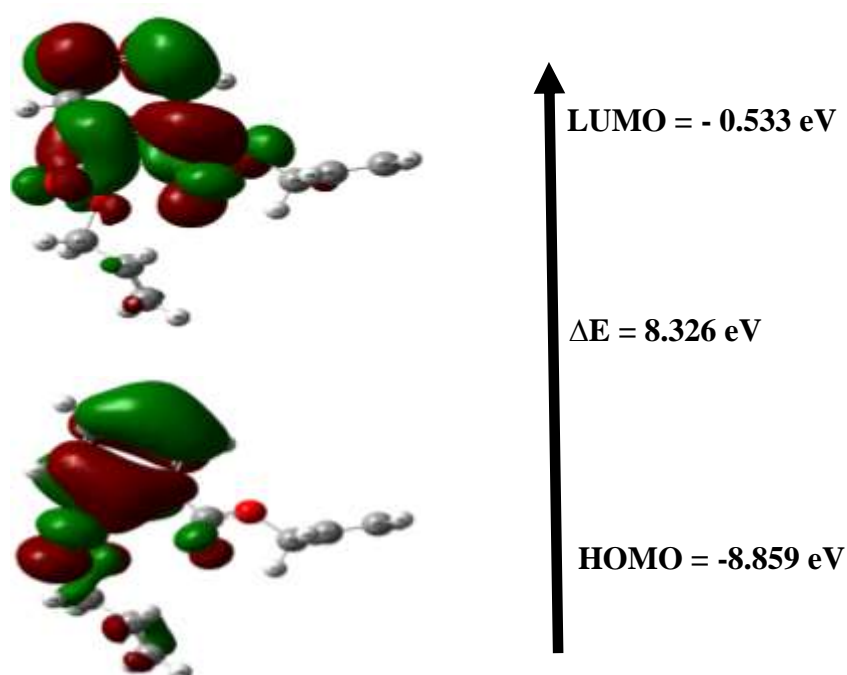


Fig 3.10: The HOMO and LUMO for the DAP using the CAM-B3LYP

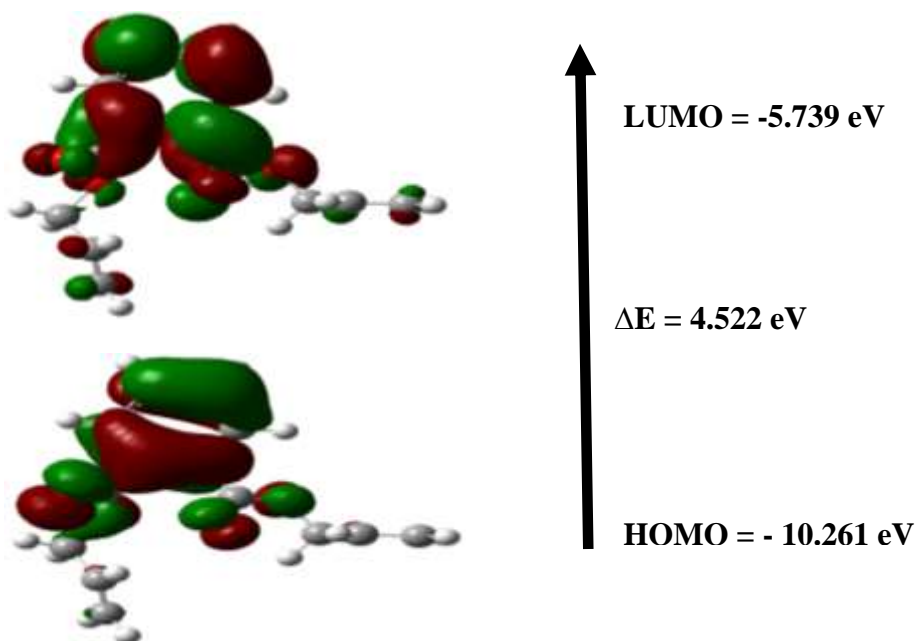


Fig 3.11: The HOMO and LUMO for DAP using the HF method.

The HOMO and LUMO results show that the energy gap using DFT is more significant than HF, which indicates that no charge transfer occurs within the molecule, and the structure is more stable with the DFT. The high stability, in turn, shows low chemical reactivity. The energy gap between HOMO and LUMO has been used to prove the bioactivity of the molecule. A large gap also indicates that the molecule is less polarized and is known as a hard molecule, and it implies high stability being less chemical reactivity.

Table 3.5: The HOMO, LUMO, and energy gap for the DAP using the DFT and HF methods.

	HF	DFT
LUMO	-5.739 eV	- 0.533 eV
HOMO	- 10.261eV	- 8.859 eV
Energy gap	4.522 eV	8.326 eV

3.6.3 Ionization Potential (I) and Electron Affinity (A)

It is clear from chapter two 2.10.2, 2.10.3 that these two parameters related directly to HOMO and LUMO energies. The high ionization energy means low chemical reactivity and vis versa. The increasing electron affinity indicates increasing the ability to gain electrons, which means a better electron acceptor. The Table 3.6 shows that the ionization potentials are 8.859 and 10.261 eV for the DFT and HF methods, respectively. It is noticed that the ionization potential energy at the DFT is lower than that of the HF method. The values of electron affinity are 0.533 and 5.739 eV at the DFT and HF, respectively.

3.6.4 Global hardness (η) and Global Softness (S)

The principles of hardness and softness will help to understand the behavior of chemical systems. Its hardness controls the ability of a molecule to polarize, while softness is the inverse of hardness and measures the degree of charge transfer within the molecule. Molecules with a higher hardness value are less reactive and more stable than soft ones in terms of reactivity [104]. Table 3.6 shows that the global hardness value for the DFT is higher than that for the HF method, with values of 4.163 eV and 2.261 eV. In addition, the values of softness are 0.240 and 0.442 eV, respectively. The high hardness and low softness of the DFT compared with the HF reveals that the system is more stable with the DFT method. In general, it can be said that the increase in softness increases chemical reactivity and increase in hardness decreases chemical reactivity.

3.6.5 Electronegativity (χ) and Electrophilicity (ω)

Electronegativity is a chemical characteristic that determines the likelihood of an atom attracting a shared pair of electrons in a covalent bond. It is an important feature because it allows atoms to link together. This creates two poles of positive and negative charge on the sharing atoms, resulting in a polarized bond. A high value of electronegativity indicates the better acceptor electron molecule.

Electrophilicity index (ω) measures the energy reduction of a molecule due to electron stream between the donor and the acceptor. A higher electrophilic index indicates better electron acceptor, while a lower electrophilic index indicates better electron donor.

The calculated electronegativity values listed in Table 3.6 show that the higher value is 8.0 eV for the HF while it has 4.696 eV for the CAM B3LYP. It is noted that the value of electronegativity of the HF is twice those of the DFT. This is due to the direct link of electronegativity with ionization potential and electron affinity (HOMO and LUMO). In the case of the DFT, HOMO and LUMO are affected by the exchange-correlation term, which relies on the magnitude of the electronic density. The values of electrophilicity are 2.648 and 14.153 eV for the DFT and HF methods, respectively, as shown in Table 3.6.

3.6.6 Chemical Potential (ρ)

The quantity of energy received or released during a chemical reaction is referred to as chemical potential. Electronegativity is the negative of this property. Table 3.6 shows the values of the chemical potential, they are -4.696 and -8.000 eV for both the DFT and HF methods.

Table 3.6: The electronic molecular properties of the DAP monomer using the DFT and HF methods.

Parameters	CAM B3LYP	HF
Total energy (Hartree)	-842.614	-837.954
Ionization potential (I) (eV)	8.859	10.261
Electron affinity (A) (eV)	0.533	5.739
Global hardness (η) (eV)	4.163	2.261

Global softness (s) (eV)⁻¹	0.240	0.442
Electronegativity (χ) (eV)	4.696	8.000
Electrophilicity index (ω) (eV)	2.648	14.153
Chemical potential (ρ) (eV)	-4.696	-8.000

The energy gap alone is not sufficient to express the stability of the molecule; the electronic properties can tell if the compound can react or not. For example, if the hardness is high, the molecule is stable, leading to a solid aromatic structure.

3.6.7. Polarizability and First Order Hyperpolarizability Calculations

Higher dipole moment, polarizability, and first-order polarizability values are significant for more active NLO characteristics. These properties with their components have been calculated using the CAM B3LYP and HF methods with the 6-311+G(d,p) basis set in the gas phase. The obtained results have been converted from atomic units (a.u.) into electronic units (esu) using $1 \text{ a.u.} = 0.1482 \times 10^{-24} \text{ esu}$ for α and $1 \text{ a.u.} = 8.6393 \times 10^{-33} \text{ esu}$ for β . Table 3.7 shows that the values of the total dipole moment, anisotropy of polarizability and average hyperpolarizability using the DFT and HF methods. For the DFT, the values are 3.3939 Debye, $3.036 \times 10^{-24} \text{ esu}$, and $475.878 \times 10^{-33} \text{ esu}$, respectively. The average hyperpolarizability is considered significant when its value 11 times larger than Urea, and the compound is an excellent candidate to be NLO material. The significant β_{xxx} value suggests that charge delocalization occurs along the bond axis. In addition, the sigma orbitals are involved in the intramolecular charge transfer process. Figures 3.12 and 3.13 represent the relations between the polarizability and hyper polarizability with their components calculated using the DFT and HF methods.

Table 3.7: The dipole moments, polarizabilities, and first hyper polarizabilities of DAP by the DF and HF methods.

Parameter	CAM B3LYP	HF
Dipole moment		
μ_x	1.9152	-2.0752
μ_y	1.3452	-1.2426
μ_z	-2.4579	-2.7549
$\mu(\text{Debye})$	3.3939	3.6661
Polarizability in esu. (x 10⁻²⁴)		
a_{xx}	-14.198	-14.250
a_{xy}	-0.458	-0.365
a_{yy}	-13.687	-13.540
a_{xz}	0.724	-0.783
a_{yz}	0.467	-0.412
a_{zz}	-16.426	-16.439
\bar{a}	-14.770	-14.743
$\Delta\alpha$	3.036	3.098
Hyperpolarizability in esu (x 10⁻³³)		
β_{xxx}	347.748	-390.153
β_{xxy}	99.985	-9.787
β_{xyy}	-199.312	186.727
β_{yyy}	158.455	-238.174
β_{xxz}	-158.406	-197.252

β_{xyz}	-62.461	-65.838
β_{yyz}	-143.430	-122.485
β_{xzz}	160.916	-149.262
β_{yzz}	-99.950	151.922
β_{zzz}	-23.191	-33.031
$\langle\beta\rangle$ (esu)	475.878	507.993

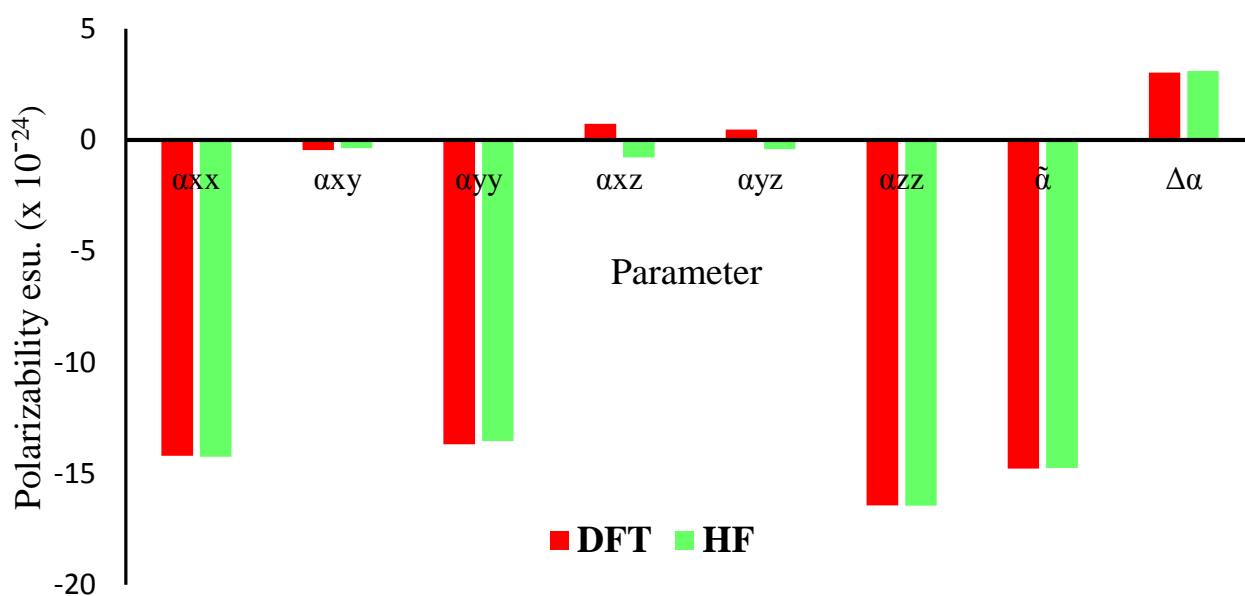


Fig 3.12: Components and total values of polarizability in the CAM B3LYP and HF methods.

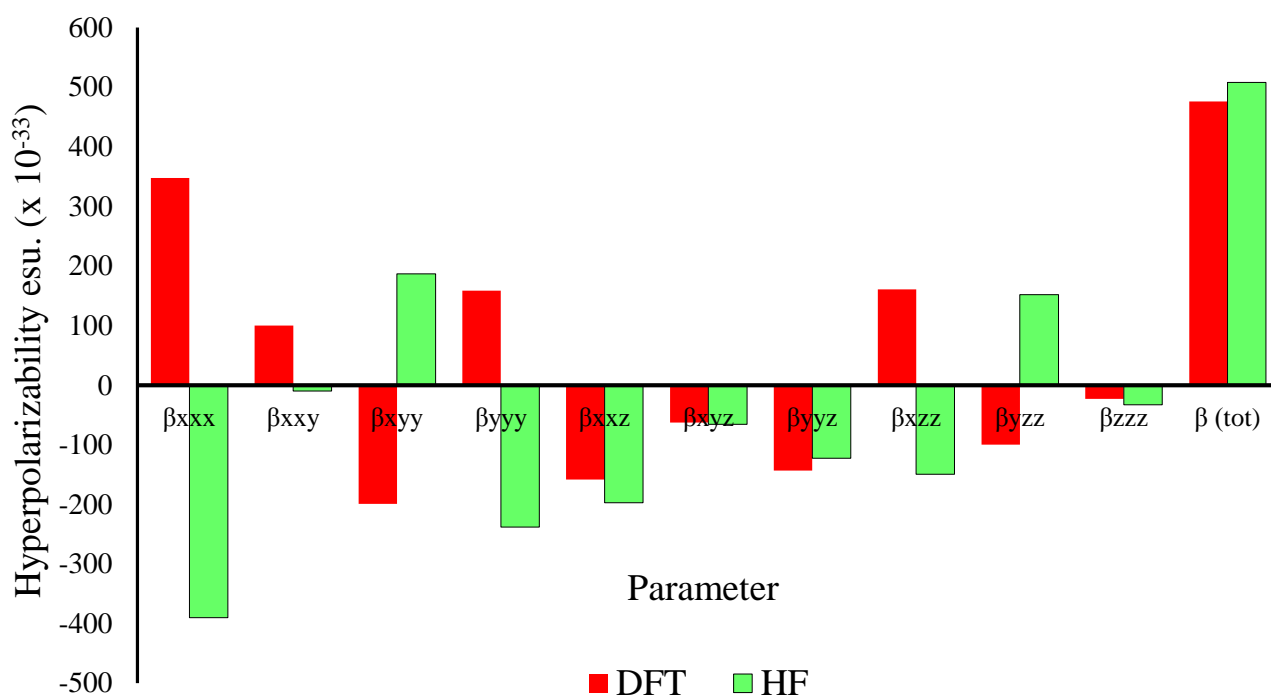


Fig 3.13: Components and total values of hyperpolarizability in CAM B3LYP and HF methods.

3.7 Spectroscopy

3.7.1 Vibrational Frequencies

Vibrational spectrum of an organic compound is requisite in establishing the identity of the compound. When the molecules of the material absorb infrared rays, a spark occurs to the material atoms as a result of this energy. This fluctuation is in the form of a vibration of the atoms, that is, a vibrational transfer of the atoms to each other occurs in the molecule. It leads to a periodic change in the length of the chemical bonds, or a change in the angles between the chemical bonds in the molecule. Each vibrational movement may result from the movement of two atoms or may include group of atoms.

The wavelength or frequency at which this absorption occurs depends on the atoms mass, strength of the bonds (constant of the force of bond) that make up the molecule as shown in eq 3.1. , and geometry of the position of the atoms in the molecule [106, 107]. The number of vibrational transitions in the case of nonlinear particles is $3N-6$ [108]. Hence, for our molecule there is 90 vibrational frequencies because it consists of 32 atoms.

$$\nu = \frac{1}{2\pi} \sqrt{\frac{K}{\mu}} \quad (3-1)$$

Where: k is the elasticity constant or the bond strength constant.

μ : is the reduced mass, and given by:

$$\mu = \frac{m_1 m_2}{m_1 + m_2} \quad (3-2)$$

Where: m_1, m_2 is the atomic mass of atoms x_1, x_2 .

One of the important goals of this work is to high light and separate the different types of molecular motion (the movement of the molecule corresponds to a specific frequency of vibration). DFT with hybrid functions CAM B3LYP and HF methods with the 6-311+G (d, p) basis set have been used to determine the modes of vibration of the DAP molecule. IR Spectrum for the DAP molecular system does not have an imaginary frequency in which that a sign to the validity of the relaxation and stability nature of the molecular system. The calculated IR and Raman wavenumbers through the [3500-500] are scaled by the scaling factor of 0.9679. Figures 3.14-15, and 3.17-18 show the theoretical spectrums of the DAP using the DFT and HF methods, respectively. Moreover, Figures 3.16 [14] and 3.19 [109], represent the experimental values for both the IR and Raman techniques. It is important to mention here that the VEDA program [110], is used to analyze and assign the type of vibrations.

3.7.1.1 C-H Vibrations

In general, the C-H stretching vibrations of the phenyl ring are expected in the region (3100 – 3000) cm^{-1} . The bands identified in the region (1200-1000) and (1000-700) cm^{-1} are pertaining to in-plane and out-of-plane ring C-H bending vibrations [111].

The C-H stretching of the methylene (CH_2) group falls generally at lower frequencies than that of the aromatic C-H stretching vibrations. The CH_2 asymmetric stretching modes are expected in the region (3000-3100) cm^{-1} while symmetric CH_2 stretch will be observed between (2900 and 3000) cm^{-1} [112, 113].

The theoretical IR and Raman of the DAP molecular system shown in Figures 3.14, 3.15 and 3.17, 3.18 declares the wavenumber versus the intensity of each mode. Figures show that the C-H stretching vibrations on benzene ring are in the region (3093-3127) cm^{-1} at CAM B3LYP and (3223-3266) cm^{-1} at HF method, while the experiment value is 3076 cm^{-1} . As expected, all the C-H bands are pure stretching modes. The DFT value is closer to the experimental one. It is worth noting that these stretching vibrations are weak in intensity for the IR spectrum while they are strong in intensity for the Raman spectrum. The C-H bending vibrations on the benzene ring are observed in the range of values from (1044-1494) and (1204-1544) cm^{-1} for DFT and HF methods, respectively.

For DFT method, the CH_2 stretching modes are found to be in the range from 2994-3135 cm^{-1} ($\text{H}_{31}\text{-C}_{18}\text{-H}_{32}$, $\text{H}_{25}\text{-C}_{14}\text{-H}_{26}$) / 2994-3133 cm^{-1} ($\text{H}_{29}\text{-C}_{17}\text{-H}_{30}$, $\text{H}_{23}\text{-C}_{13}\text{-H}_{24}$). In the HF method, these vibrations are found to be from (3135-3257/3134-3257) cm^{-1} . The experimental result 2940 cm^{-1} for IR [114] and 3027 cm^{-1} for Raman will give the preference for the DFT over the HF method.

3.7.1.2 C=O Vibrations

The double bond of this stretching vibration arises from the difference in electronegativity for the carbon and oxygen atoms. The oxygen atom has electronegativity higher than carbon, and this leads to form two poles and a solid double bond with a high degree of coupling. The carbonyl C=O stretching mode is expected to occur in the region (1750-1600) cm^{-1} [115]. Figures 3.14-15 reveal that this mode occurs at the value of (1752/1766) and (1895/1907) cm^{-1} for the DFT and HF methods, respectively. The experimental value of this mode is 1729 cm^{-1} for IR and 1730 cm^{-1} for Raman. These values can be reached by the DFT method. From Figures, it can be seen that the intensity of this band is strong for the IR spectrums and weak for Raman ones.

3.7.1.3 =CH Arene Vibrations

The =CH stretching vibration on arene (C=C) was (1648/1648) cm^{-1} and (1372, 1785/ 1376, 1785) cm^{-1} for the DFT and HF methods. The results of the DFT have good agreement with the experimental value 1649 and 1651 cm^{-1} for the IR and Raman techniques.

3.7.1.4 C=C Aromatic Vibrations

The C=C stretching vibrations of the aromatic ring are extremely essential in the spectrum of aromatic compounds and are highly distinctive of the aromatic ring itself. In general, bands appear in the region (1400-1650) cm^{-1} are assigned to the benzene ring vibrations [116]. In this work, the C=C stretching vibrations on benzene were observed at the range from (1044-1625) and (1095-1730) cm^{-1} for DFT and HF methods, respectively. The measured values of this mode were 1580 and 1600 cm^{-1} for IR and 1581 and 1603 cm^{-1} for the Raman.

3.7.1.5 C-O-C Vibrations

The C-O-C stretching vibrations for the DAP molecule have been observed at 1296, 1136, and 1076 cm^{-1} for the DFT and 1404, 1216, and 1149 cm^{-1} for the HF method. The experimental values were 1277, 1125, and 1071 cm^{-1} for the IR and 1276, 1169, and 1043 cm^{-1} for Raman technique, they have good agreement with the DFT method.

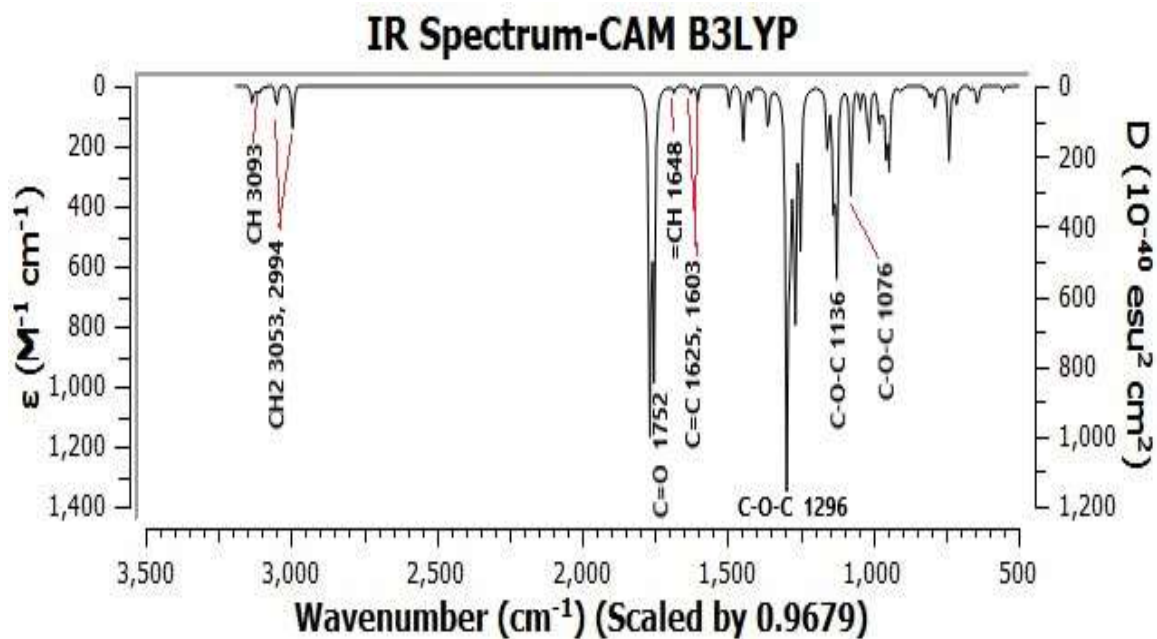


Fig 3.14: The IR spectrum for the DAP using the CAM B3LYP method.

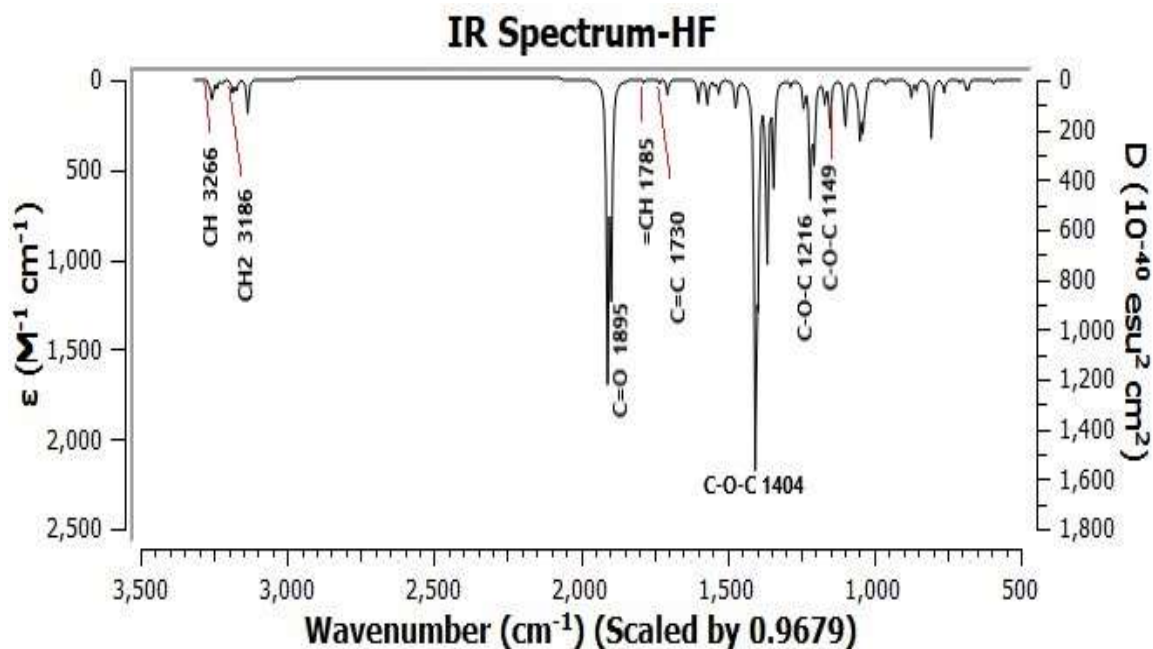
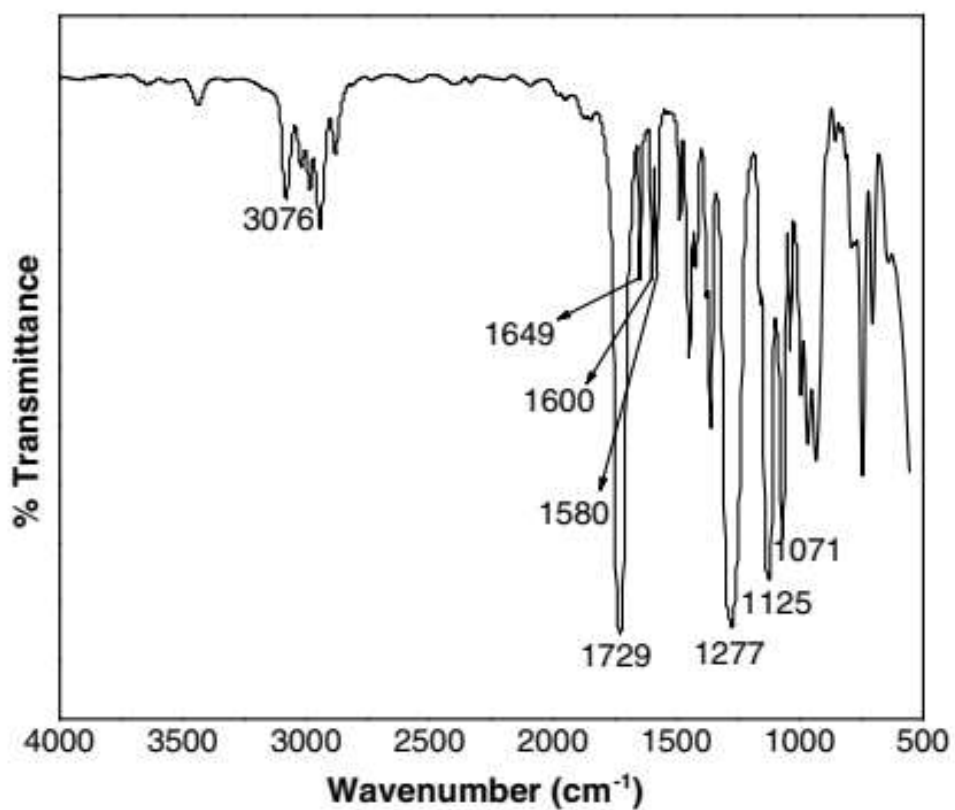


Fig 3.15: The IR spectrum for the DAP using the HF method.



IR frequency/cm ⁻¹	Attribution
3076	CH stretching vibration on benzene
1729	C=O stretching vibration
1649	=CH stretching vibration on arene
1580, 1600	C=C stretching vibration on benzene
1071, 1125, 1277	C-O-C stretching vibration

Fig 3.16: Experimental FT-IR spectrum of DAP [14].

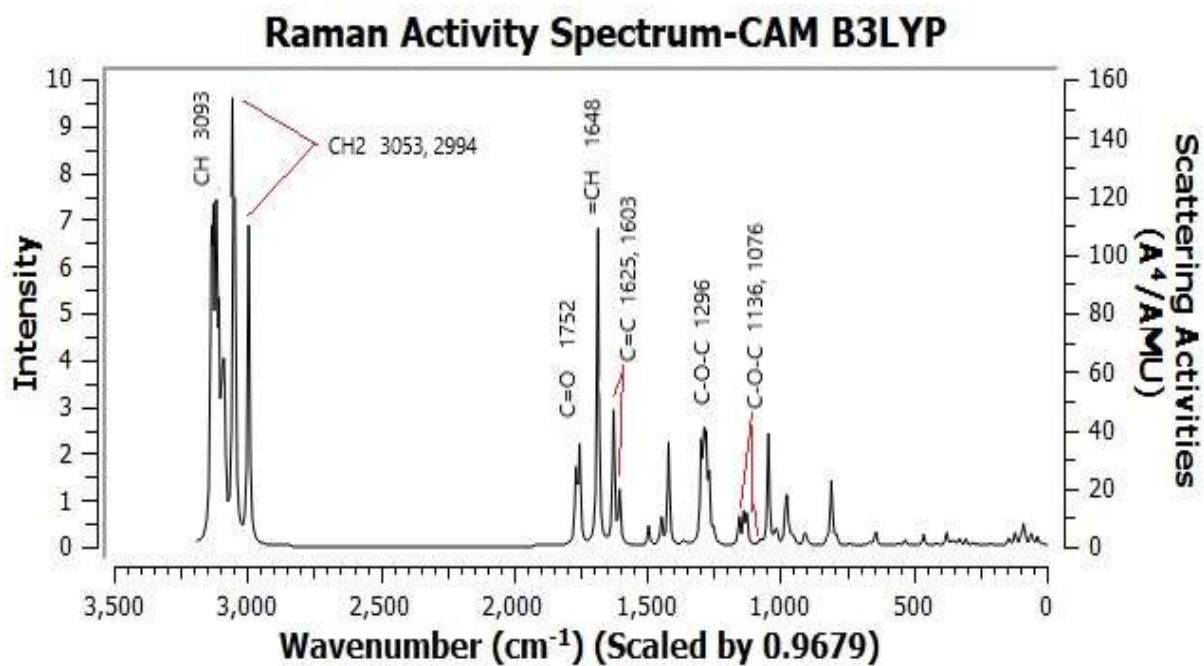


Fig 3.17: The Raman spectrum for the DAP using the CAM B3LYP method.

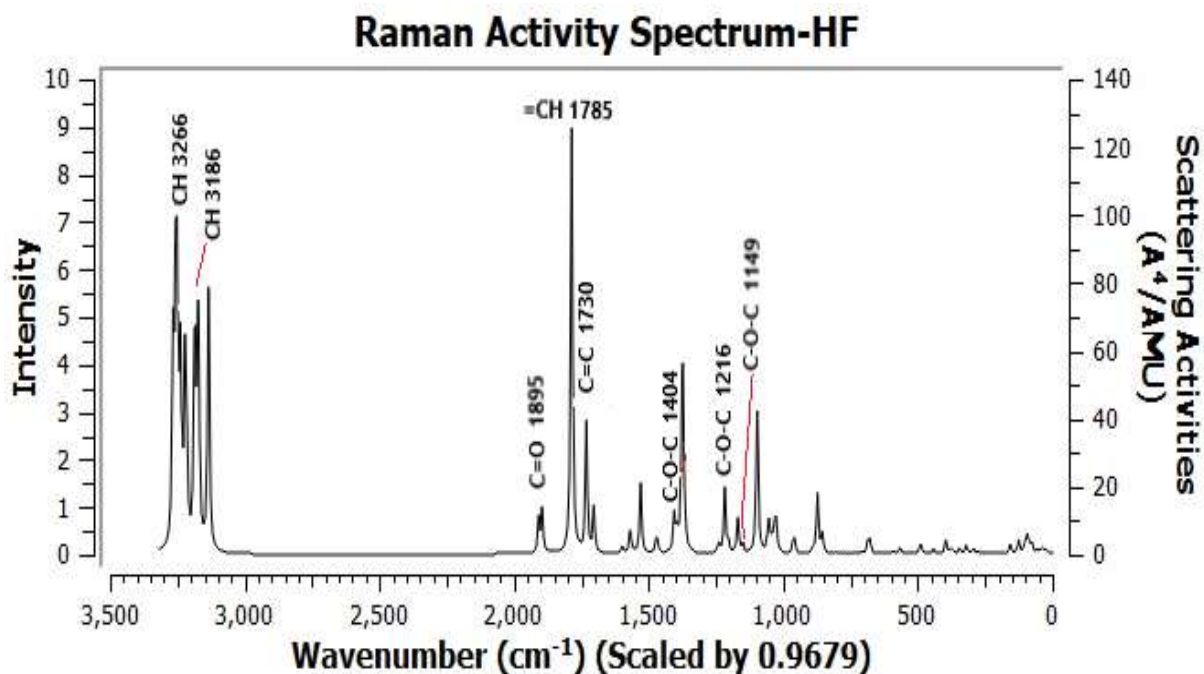


Fig 3.18: The Raman spectrum for the DAP using the HF method.

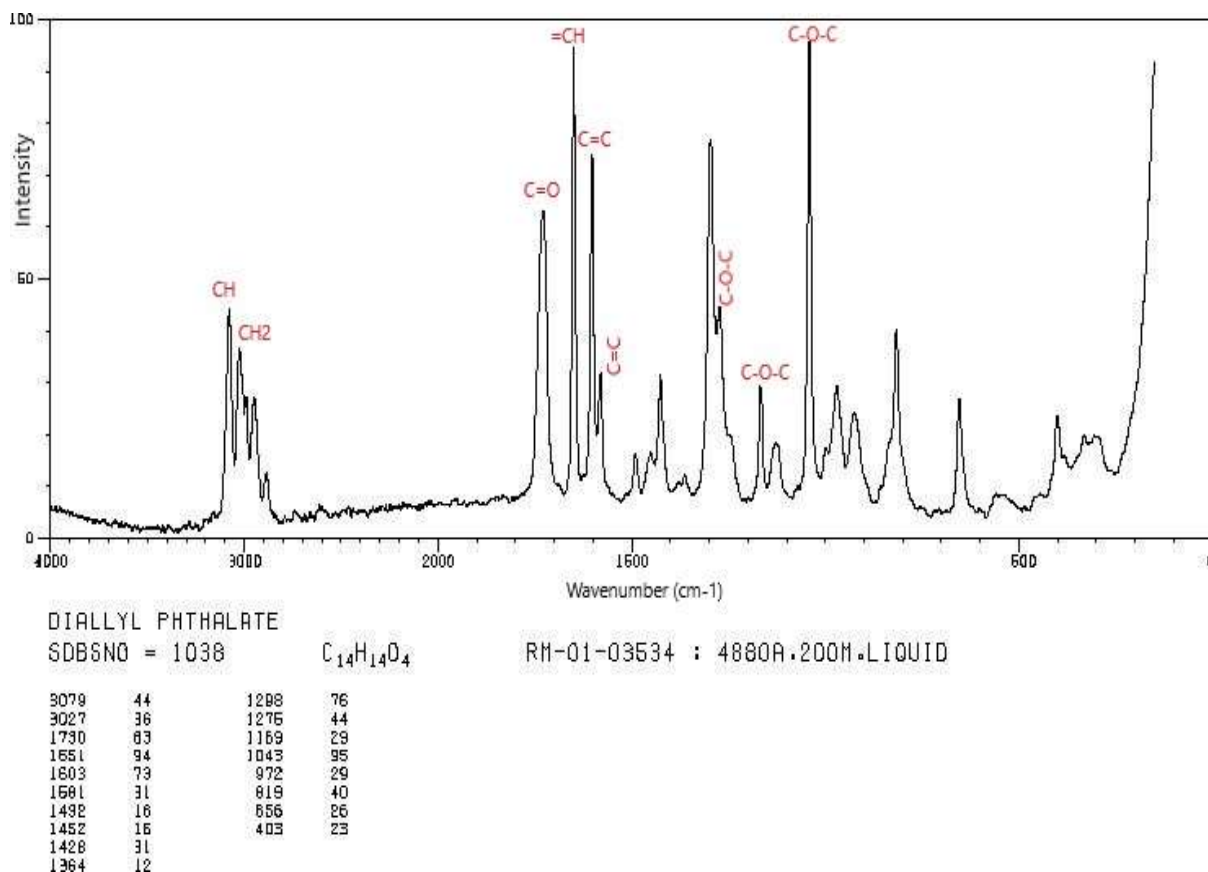


Fig 3.19: Experimental Raman spectrum of the DAP [109].

Figures 3.17-18 shows the Raman spectrum of DAP structure molecule. The results show a great convergence between our results and the experimental results. The value of C-H₂ vibrations is (2994.44, 3133.90) cm⁻¹ at CAM B3LYP and HF respectively, while the experiment value is 2950 cm⁻¹. The value of C=O vibrations is (1766.82, 1908.04) cm⁻¹ at CAM B3LYP and HF respectively, while the experiment value is 1800 cm⁻¹. The value of C=C Aliphatic vibrations is

(1684.12, 1785.71) cm^{-1} at CAM B3LYP and HF respectively, while the experiment value is 1602 cm^{-1} . The value of C=C Aromatic vibrations is (1494.06, 1544.38) cm^{-1} at CAM B3LYP and HF respectively, while the experiment value is 1450 cm^{-1} . The value of C-O vibrations is (1277.80, 1216.95) cm^{-1} at CAM B3LYP and HF respectively, while the experiment value is 1290 cm^{-1} . The value of C-C Aromatic vibrations is (1044.09, 1059.69) cm^{-1} at CAM B3LYP and HF respectively, while the experiment value is 960 cm^{-1} [114].

3.8 Conclusions and future work

3.8.1 Conclusions

In this study, the density functional theory and Hartree-Fock methods have been used to investigate the DAP molecule. The results were obtained using Gaussian 09 program and visualized with Gauss View 06. The Veda Program has been used to analyze and identify the different modes of vibrations. According to these results, it can be concluded that:

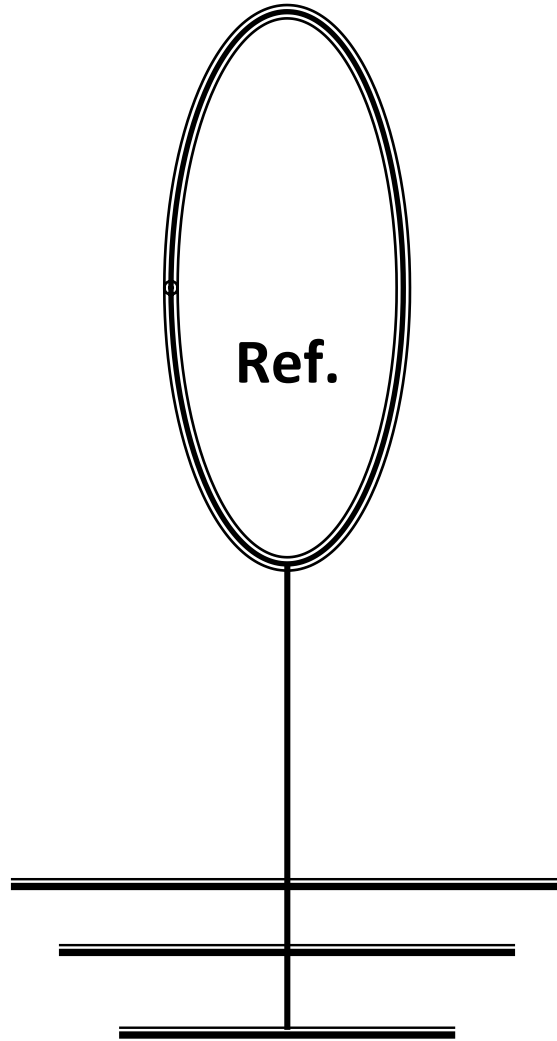
1. The potential energy surface scan technique is a powerful and necessary tool to prepare the geometry of molecule before subjected it to the full optimization.
2. The CAM B3LYP method leads to a converged molecule with minimum energy equal to -842.614348 Hartree compared with -837.953983 Hartree of the HF method.
3. The results show that the bond lengths calculated using DFT-CAM B3LYP are better than those found using the HF method. The correlation factors were 0.949 and 0.946 for the DFT and HF, respectively.
4. The lone pairs and double bonds of the oxygen atoms O₃ and O₄ are responsible for the short bond angles O₁-C₁₁-C₅ and O₂-C₁₂-C₆. They lead to higher electron density, solid repulsive force and then distorted angles.
5. The planarity of the benzene ring makes all the dihedral angles are about zero.
6. Because of the electronegativity of the oxygen all the oxygen atoms (O₁, O₂, O₃, and O₄) have negative and similar values.
7. It is noticed that all the hydrogen atoms in the molecule are positive with similar values, which comes from hydrogen's ability to give its electron.
8. The value of the energy gap using the DFT reveals that the molecule has higher chemical stability. It was 8.326 and 4.522 eV for the DFT and HF methods.

9. The results of the IR and Raman techniques refer to good agreement between the calculated results using the DFT and the experimental ones.

3.8.2 Future works

1. Study the adhesive property of the DAP resins with metal after blended with epoxy resins.
2. Study the optical and electronic properties of the polybutylene terephthalate using the DFT method with Quantum espresso or MOPAC software.
3. Investigate the adhesion of polyimides with some metals such as Aluminium.

References



References

1. Young, R.J. and P.A. Lovell, Introduction to polymers. 2011: CRC press.
2. Bergman, S.D. and F. Wudl, Mendable polymers. *Journal of Materials Chemistry*, 2008. **18**(1): p. 41-62.
3. Patton, L., CPSC staff toxicity review of two phthalates and one phthalate alternative for consideration by the Chronic Hazard Advisory Panel, 2011. US Consumer Product Safety Commission, Bethesda, MD, 2011.
4. Takeuchi, S., Differential effects of phthalate esters on transcriptional activities via human estrogen receptors α and β , and androgen receptor. *Toxicology*, 2005. **210**(2-3): p. 223-233.
5. <https://www.bing.com/images/search?q=Phthalates+Chemical+Formula&form=IRBPRS&first=1&tsc=>
6. Dbira, S., Degradation of diallyl phthalate (DAP) by fenton oxidation: mechanistic and kinetic studies. *Applied Sciences*, 2018. **9**(1): p. 23.
7. He, S., Mechanical and thermal properties of bisphenol A-based cyanate ester and diallyl phthalate blends. *Polymer bulletin*, 2009. **62**(2): p. 237-246.
8. Gu, A., Thermal and mechanical performances of diallyl phthalate/clay nanocomposites. *Polymer-Plastics Technology and Engineering*, 2006. **45**(8): p. 957-961.
9. Usmani, A. and I. Salyer, New flexibilized diallyl phthalate resins for encapsulating electronic display devices. *Journal of Materials Science*, 1981. **16**(4): p. 915-926.
10. Ohtsuka, K., Preparation and properties of cured diallyl phthalate resin modified with dimeric acid polyamide derivatives. *Journal of Applied Polymer Science*, 2012. **126**(S2): p. E218-E224.
11. Ohtsuka, K., Properties of novel diallyl phthalate resin modified with sulfur-containing allyl ester compounds. *Polymer international*, 2014. **63**(4): p. 752-759.
12. Yoshioka, T., Fission-fragment registration and etching properties of diallyl phthalate with reference to its use as an external detector in fission-track dating. *Nuclear Instruments and Methods in Physics Research Section B: Beam Interactions with Materials and Atoms*, 2003. **207**(3): p. 323-332.
13. Tondi, G., A. Kandelbauer, and S.H. Goodman, Allyls, in *Handbook of Thermoset Plastics*. 2014. p. 173-189.
14. Xu, S.-A., Effect of ultrasonic separation on the structure and properties of diallyl phthalate prepolymer. *Ultrasonics sonochemistry*, 2008. **15**(4): p. 364-369.
15. Haward, R., Polymerization of diallyl phthalate. *Journal of Polymer Science*, 1954. **14**(78): p. 535-545.
16. Heydel, C., P. Cassagnau, and A. Michel, Bulk crosslinking of diallyl phthalate monomers. *Journal of Rheology*, 1999. **43**(3): p. 499-519.
17. Tsuruta, T., Diallyl phthalate resin and its copolymers containing allyl diglycol carbonate as nuclear track detectors. *Radiation measurements*, 2000. **32**(4): p. 289-297.
18. Yoshioka, T., Radioactivity of neutron-irradiated materials used for fission track dating—improvement on dating procedures to eliminate radiation exposure by using a diallyl phthalate detector. *Radiation measurements*, 2006. **41**(5): p. 513-519.
19. Gerbaux, P., Metastable dimethyl phthalate molecular ions: Does the loss of a methoxyl radical proceed with or without anchimeric assistance? *International Journal of Mass Spectrometry*, 2010. **290**(2-3): p. 127-132.
20. Jeilani, Y.A., B.H. Cardelino, and V.M. Ibeanusi, Density functional theory and mass spectrometry of phthalate fragmentations mechanisms: modeling hyperconjugated

- carbocation and radical cation complexes with neutral molecules. *Journal of the American Society for Mass Spectrometry*, 2011. **22**(11).
21. Yadav, P.S. and D.K. Pandey, A DFT study for the structural and electronic properties of Zn_mSe_n nanoclusters. *Applied Nanoscience*, 2012. **2**(3): p. 351-357.
 22. Şen, F. and B. Göker, A theoretical investigation b monomer that is a plastic pol manufacture of eyeglass lens. *American Journal of Optics and Photon*, 2014. **2**(1): p. 7-11.
 23. Ridha, S.M., Z.A. Saleh, and F.W. Askar, Theoretical and Experimental Study for FT-IR and UV/VIS Spectra of 1, 4-diphenyl-3-(phenylammonio)-1H-1, 2, 4-triazolium (inner salt) by Using DFT Approach. *Physical Chemistry*, 2015. **5**(1): p. 6-15.
 24. Xu, T., Development of prediction models on base-catalyzed hydrolysis kinetics of phthalate esters with density functional theory calculation. *Environmental science & technology*, 2019. **53**(10): p. 5828-5837.
 25. Nageswari, G., Molecular analyses using FT-IR, FT-Raman and UV spectral investigation; quantum chemical calculations of dimethyl phthalate. *Journal of Molecular Structure*, 2019. **1195**: p. 331-343.
 26. Al-Owaedi, O.A.A., *Electronic Properties of Nano and Molecular Quantum Devices* Lancaster University, 2016.
 27. Pople, J.A. and D.L. Beveridge, *Molecular orbital theory*. CO., NY, 1970.
 28. Capelle, K., A bird's-eye view of density-functional theory. *Brazilian journal of physics*, 2006. **36**: p. 1318-1343.
 29. Hamerka, H.F., *Quantum mechanics: a conceptual approach*. 2004: John Wiley & Sons.
 30. Röthlisberger, P.U., *Introduction to Electronic Structure Methods*. EPFL, Lausanne, 2014.
 31. Lewars, E.G., *Molecular mechanics*, in *Computational Chemistry*. 2016, Springer. p. 51-99.
 32. Selman, S.R., *The Electronic Structure of Cubic Silicon Carbide Nanocrystals using Ab-initio Large Unit Cell Method*. University of Babylon, 2010.
 33. Wiberg, K.B., *Ab Initio Molecular Orbital Theory* by WJ Hehre, L. Radom, P. v. R. Schleyer, and JA Pople, John Wiley, New York, 548pp. Price: \$79.95 (1986). 1986, Wiley Online Library.
 34. Zielinski, T.J., *Introducing JCE LivTexts: Physical Chemistry*. Monmouth University, 2005.
 35. Hartree, D.R. The wave mechanics of an atom with a non-Coulomb central field. Part I. Theory and methods. in *Mathematical Proceedings of the Cambridge Philosophical Society*. 1928. Cambridge university press.
 36. Fock, V., Näherungsmethode zur Lösung des quantenmechanischen Mehrkörperproblems. *Zeitschrift für Physik*, 1930. **61**(1-2): p. 126-148.
 37. Zhou, D., *An Introduction of Density Functional Theory and its Application*. Physics. Drexel. Edu, 2007.
 38. Pauli, W., On the connexion between the completion of electron groups in an atom with the complex structure of spectra. *Zeitschrift für Physik*, 1925. **31**: p. 765.
 39. Szabo, A. and N.S. Ostlund, *Modern quantum chemistry: introduction to advanced electronic structure theory*. 2012: Courier Corporation.
 40. Young, D.C., *A practical guide for applying techniques to real-world problems*. *Computational Chemistry*, New York, 2001. **9**: p. 390.
 41. Ahmed, J.T.m., *Density Function Theory Calculations For donor-bridge-accepter molecular systems*. University of Babylon, 2014.
 42. Gale, J.D., *Semi-empirical methods as a tool in solid-state chemistry*. *Faraday Discussions*, 1997. **106**: p. 219-232.

43. Profeta, S., Molecular Modeling. Kirk- Othmer Encyclopedia of Chemical Technology, 2000: p. 1-46.
44. Young, D., Computational chemistry: a practical guide for applying techniques to real world problems. 2004: John Wiley & Sons.
45. Stewart, J.J., Optimization of parameters for semiempirical methods II. Applications. Journal of computational chemistry, 1989. **10**(2): p. 221-264.
46. Thiel, W., Semiempirical quantum–chemical methods. Wiley Interdisciplinary Reviews: Computational Molecular Science, 2014. **4**(2): p. 145-157.
47. Bauschlicher Jr, C.W. and H. Partridge, A modification of the Gaussian- 2 approach using density functional theory. The Journal of chemical physics, 1995. **103**(5): p. 1788-1791.
48. Labanowski, J.K. and J.W. Andzelm, Density functional methods in chemistry. 2012: Springer Science & Business Media.
49. Hohenberg, P. and W. Kohn, Inhomogeneous electron gas. Physical review, 1964. **136**(3B): p. B864.
50. Kohn, W. and L.J. Sham, Self-consistent equations including exchange and correlation effects. Physical review, 1965. **140**(4A): p. A1133.
51. Sham, L. and W. Kohn, One-particle properties of an inhomogeneous interacting electron gas. Physical review, 1966. **145**(2): p. 561.
52. Yang, W. and P.W. Ayers, Density-functional theory, in Computational Medicinal Chemistry for Drug Discovery. 2003, CRC Press. p. 103-132.
53. Burke, K., J. Werschnik, and E. Gross, Time-dependent density functional theory: Past, present, and future. The Journal of chemical physics, 2005. **123**(6): p. 062206.
54. Kohn, W., Nobel Lecture: Electronic structure of matter—wave functions and density functionals. Reviews of Modern Physics, 1999. **71**(5): p. 1253.
55. Parr, R.G. and W. Yang, Density-Functional Theory of Atoms and Molecules, vol. 16 of International series of monographs on chemistry. 1989, Oxford University Press, New York.
56. Runge, E. and E.K. Gross, Density-functional theory for time-dependent systems. Physical Review Letters, 1984. **52**(12): p. 997.
57. Alnasrawi, H.A.R., Theoretical investigation of electronic structure properties of doped zinc oxide nanosheet. University of Kerbala – College of Science, 2019.
58. Hohenberg, P. and W. Kohn, Inhomogeneous Electron Gas Phys. Rev. 136. B864, 1964.
59. Cohen, M.H., Total energy density as an interpretative tool. The Journal of Chemical Physics, 2000. **113**(8): p. 2990-2994.
60. Weis, J., H. Schäfer, and G. Schön, Neue ternäre Telluride und Selenide der Alkalimetalle mit Elementen der 3. Hauptgruppe. Zeitschrift für Naturforschung B, 1976. **31**(10): p. 1336-1340.
61. Dihe, A.A., Theory Of Electron Transport Through Single Molecules. Lancaster University, 2017.
62. Hood, R.Q., Exchange and correlation in silicon. Physical Review B, 1998. **57**(15): p. 8972.
63. Winterrose, M.L., Quantum Mechanical Simulation and X-Ray Scattering Applied to Pressure-Induced Invar Anomaly in Magnetic Iron Alloy. California Institute of Technology Pasadena, California, 2011.
64. Reel, J., A comparative review of computational methods as applied to gold(I) complexes and mechanisms Department of Chemistry Duke University, 2016.
65. AL-Shimmari, A.J.N., Density Functional Theory and Semiempirical Investigations to study Amino-,and Methyl-Benzene Molecules. University of Babylon 2011.

66. Kim, K. and K. Jordan, Comparison of density functional and MP2 calculations on the water monomer and dimer. *The Journal of Physical Chemistry*, 1994. **98**(40): p. 10089-10094.
67. Yanai, T., D.P. Tew, and N.C. Handy, A new hybrid exchange–correlation functional using the Coulomb-attenuating method (CAM-B3LYP). *Chemical physics letters*, 2004. **393**(1-3): p. 51-57.
68. Cai, Z.-L., K. Sendt, and J.R. Reimers, Failure of density-functional theory and time-dependent density-functional theory for large extended π systems. *The Journal of chemical physics*, 2002. **117**(12): p. 5543-5549.
69. Li, M., Accurate prediction of the properties of materials using the CAM- B3LYP density functional. *Journal of Computational Chemistry*, 2021. **42**(21): p. 1486-1497.
70. Slov, A.C., Book Review: Exploring Chemistry with Electronic Structure Methods, James B. Foresman and AEleen Frisch. Published by Gaussian, Inc., Pittsburgh, PA, 15106 USA. 354 pages. Soft cover: \$42.00 ISBN 0-9636769-3-8, Hard cover: \$100.00 ISBN 0-9636769-4-6 Abraham F. Jalbout. *Acta Chim. Slov*, 2003. **50**: p. 159-160.
71. Zener, C., Analytic atomic wave functions. *Physical Review*, 1930. **36**(1): p. 51.
72. Slater, J.C., Atomic shielding constants. *Physical Review*, 1930. **36**(1): p. 57.
73. Mueller, M.R., *Fundamentals of quantum chemistry: molecular spectroscopy and modern electronic structure computations*. Vol. 265. 2001: Springer.
74. Yariv, A., *Quantum electronics*. 1989: John Wiley & Sons.
75. Larsson, P.-E., *Modelling Chemical Reactions: Theoretical Investigations of Organic Rearrangement Reactions*. 2003, Acta Universitatis Upsaliensis.
76. Mueller, M., *Fundamentals of Quantum Chemistry Molecular Spectroscopy and Modern Electronic Structure Computations*. Chemistry in Britain, 2001.
77. Huzinaga, S., *Basis sets for molecular calculations*. *Computer physics reports*, 1985. **2**(6): p. 281-339.
78. Clark, T., Efficient diffuse function- augmented basis sets for anion calculations. III. The 3- 21+ G basis set for first- row elements, Li–F. *Journal of Computational Chemistry*, 1983. **4**(3): p. 294-301.
79. Kim, B.G., Mercury-containing species and carbon dioxide adsorption studies on inorganic compounds using density functional theory. 2010: The University of Arizona.
80. Kosar, B., C.J.S.A.P.A.M. Albayrak, and B. Spectroscopy, Spectroscopic investigations and quantum chemical computational study of (E)-4-methoxy-2-[(p-tolylimino) methyl] phenol. 2011. **78**(1): p. 160-167.
81. Hizaddin, H.F., R. Anantharaj, and M.A.J.J.o.M.L. Hashim, A quantum chemical study on the molecular interaction between pyrrole and ionic liquids. 2014. **194**: p. 20-29.
82. Heidari Nezhad Janjanpour, M., et al., Study of the ionization potential, electron affinity and HOMO-LUMO gaps in the small fullerene nanostructures. 2018. **1**(2): p. 45-48.
83. Bredas, J.-L.J.M.H., Mind the gap! 2014. **1**(1): p. 17-19.
84. Bittner, E.J.U.o.H., Department of Chemistry, *Quantum Mechanics: Lecture Notes for Chemistry*. 2003.
85. Pilli, S.R., T. Banerjee, and K. Mohanty, HOMO–LUMO energy interactions between endocrine disrupting chemicals and ionic liquids using the density functional theory: Evaluation and comparison. *Journal of Molecular Liquids*, 2015. **207**: p. 112-124.
86. Raheem, A., K. Al-Shejry, and E.D.J.B.J.o.S. Al-bermany, Density Functional Theory Calculations For MethylBenzene Molecules group. 2012. **5**: p. 57-64.
87. Shenghua, L., Y. He, and J. Yuansheng, Lubrication chemistry viewed from DFT-based concepts and electronic structural principles. *International Journal of Molecular Sciences*, 2004. **5**(1): p. 13-34.

88. Mahdi, B.S., A Study OF the Electronic Structure of Azabenzen Molecules: by B3LYP-DFT Density Functional Calculation.
89. Rajalakshmi, K. and D. Nayak, HOMO–LUMO Analysis of Dasatinib. *Int. J. Mater. Sci*, 2017. **12**: p. 32-37.
90. Itskowitz, P. and M.L.J.T.J.o.P.C.A. Berkowitz, Chemical potential equalization principle: direct approach from density functional theory. 1997. **101**(31): p. 5687-5691.
91. Anantharaj, R. and T. Banerjee, Evaluation and comparison of global scalar properties for the simultaneous interaction of ionic liquids with thiophene and pyridine. *Fluid Phase Equilibria*, 2010. **293**(1): p. 22-31.
92. Ramalingam, S., Spectroscopic (infrared, Raman, UV and NMR) analysis, Gaussian hybrid computational investigation (MEP maps/HOMO and LUMO) on cyclohexanone oxime. 2012. **96**: p. 207-220.
93. Asghari-Khiavi, M., P. Hojati-Talemi, and F.J.J.o.M.S.T. Safinejad, Polarizability and first-order hyperpolarizability of cyclic imides. 2009. **910**(1-3): p. 56-60.
94. Silverstien, R., I. Webster, and D. Kiemle, spectrometric Identification of organic compounds 7 th edn. John willy and sons Inc, Nj, USA, 2005.
95. Al-aarji, N.A.-h.T.A., Electronic, Structural and Spectroscopic Properties of Aluminum Antimonide : A Density Functional Theory Study. University of Babylon, 2016.
96. Young, H.D. and R.A. Freedman, University physics with modern physics 13th edition. Haettu, 2012. **11**: p. 2020.
97. M. J. Frisch, G.W.T., H. B. Schlegel, G. E. Scuseria, M. A. Robb, J. R. Cheeseman, G. Scalmani, V. Barone, G. A. Petersson, H. Nakatsuji, X. Li, M. Caricato, A. Marenich, J. Bloino, B. G. Janesko, R. Gomperts, B. Mennucci, H. P. Hratchian, J. V. Ortiz, A. F. Izmaylov, J. L. Sonnenberg, D. Williams-Young, F. Ding, F. Lipparini, F. Egidi, J. Goings, B. Peng, A. Petrone, T. Henderson, D. Ranasinghe, V. G. Zakrzewski, J. Gao, N. Rega, G. Zheng, W. Liang, M. Hada, M. Ehara, K. Toyota, R. Fukuda, J. Hasegawa, M. Ishida, T. Nakajima, Y. Honda, O. Kitao, H. Nakai, T. Vreven, K. Throssell, J. A. Montgomery, Jr., J. E. Peralta, F. Ogliaro, M. Bearpark, J. J. Heyd, E. Brothers, K. N. Kudin, V. N. Staroverov, T. Keith, R. Kobayashi, J. Normand, K. Raghavachari, A. Rendell, J. C. Burant, S. S. Iyengar, J. Tomasi, M. Cossi, J. M. Millam, M. Klene, C. Adamo, R. Cammi, J. W. Ochterski, R. L. Martin, K. Morokuma, O. Farkas, J. B. Foresman, and D. J. Fox, Gaussian, Inc., Wallingford CT, 2016.
98. Cramer, C.J., Essentials of computational chemistry: theories and models. 2013: John Wiley & Sons.
99. Lide Jr, D.R., A survey of carbon-carbon bond lengths. *Tetrahedron*, 1962. **17**(3-4): p. 125-134.
100. Gordy, W., A relation between bond force constants, bond orders, bond lengths, and the electronegativities of the bonded atoms. *The Journal of Chemical Physics*, 1946. **14**(5): p. 305-320.
101. Vincent-Finley, R.E. A reduced basis method for molecular dynamics simulation. 2005.
102. Matczak, P., A test of various partial atomic charge models for computations on diheteroaryl ketones and thioketones. *Computation*, 2016. **4**(1): p. 3.
103. Ramalingam, S., Spectroscopic (infrared, Raman, UV and NMR) analysis, Gaussian hybrid computational investigation (MEP maps/HOMO and LUMO) on cyclohexanone oxime. *Spectrochimica Acta Part A: Molecular and Biomolecular Spectroscopy*, 2012. **96**: p. 207-220.
104. Ramalingam, A., R.K. Gurunathan, and P. Chanda Nagarajan, Investigation of Potential Azeotrope Breakers Using DFT and COSMO Approach. *ACS omega*, 2020. **5**(27): p. 16885-16900.

105. Dheivamalar, S., L. Sugi, and K. Ambigai, Density functional theory study of exohedral carbon atoms effect on electrophilicity of nicotine: comparative analysis. *Computational Chemistry*, 2016. **4**(1): p. 17-31.
106. Rouessac, F., A. Rouessac, and D. Cruch??, *Analyse chimique*. 2004: Dunod.
107. NAGAMOUTTOU, C., *Traitement thermique et caractérisation physicochimique de matériau carbonés. Rapport de stage, Centre de recherche sur la matière divisé, Université d'Orléans*, 2006.
108. Raja, M., Synthesis, spectroscopic (FT-IR, FT-Raman, NMR, UV–Visible), first order hyperpolarizability, NBO and molecular docking study of (E)-1-(4-bromobenzylidene) semicarbazide. *Journal of Molecular Structure*, 2017. **1128**: p. 481-492.
109. Diallyl phthalate(131-17-9) Raman. https://scholar.google.com/scholar?hl=en&as_sdt=0%2C5&q=Diallyl+phthalate%28131-17-9%29.
110. Jamróz, M.H., Vibrational energy distribution analysis (VEDA): scopes and limitations. *Spectrochimica Acta Part A: Molecular and Biomolecular Spectroscopy*, 2013. **114**: p. 220-230.
111. Smith, B., *Infrared spectral interpretation: a systematic approach*. 2018: CRC press.
112. Sajan, D., NIR-FT Raman and infrared spectra and ab initio computations of glycinium oxalate. *Spectrochimica Acta Part A: Molecular and Biomolecular Spectroscopy*, 2004. **60**(1-2): p. 173-180.
113. Gunasekaran, S., S. Varadhan, and K. Manoharan, Fourier Transform Infrared and Laser Raman Spectroscopic Investigations on 2-N-(Benzoylamino) Pyridine. *Indian Journal of Physics*, 1993. **67**: p. 95-101.
114. Pereira, L.A.S. and C.A.T. Sáenz, Raman and FT-IR investigation of neutron and fission-fragment irradiated DAP polymer. *Vibrational Spectroscopy*, 2019. **105**: p. 102971.
115. Barbet, F., Comparative Raman spectroscopy studies of photosensitive polymers. *Materials chemistry and physics*, 1998. **55**(3): p. 202-208.
116. Amul, B., Spectral, DFT and molecular docking investigations on Etodolac. *Journal of Molecular Structure*, 2019. **1195**: p. 747-761.

الخلاصة

في هذه الرسالة تمت دراسة الخواص التركيبية والإلكترونية للمونومر دايأليل فثاليت (DAP). وقد تم استخدام نظرية الدالة الوظيفية للكثافة (DFT) - CAM B3LYP وطريقة هارترى-فوك (HF) مع دوال الاساس 6-311+G (d, p) لمعالجة الدالة الموجية للنظام متعدد الجسيمات. كذلك تم استخدام برنامج Gaussian 09 و برنامج GaussView06 لانجاز ومعاينة الحسابات .

لقد استخدمت تقنية جهد طاقة السطح مع الطريقة شبه التجريبية PM6 للحصول على مونمر مخفض(محسن) الطاقة جزئيا, بعد ذلك تم تطبيق طريقة نظرية الدالة الوظيفية للكثافة وطريقة هارترى - فوك للحصول على مونيمر مخفض الطاقة كليا . لقد تم دراسة الخصائص التركيبية مثل اطوال الاواصر وقياسات الزوايا والزوايا ثنائية الاضلاع. وقد وجد ان معدل اطوال الاواصر لذرات الكربون في حلقة البنزين مساوية لـ 1.389 و 1.386 بوحدات الانكستروم لطريقي نظرية الدالة الوظيفية للكثافة وهارترى - فوك على التوالي, علما ان القيمة المحسوبة عالميا تساوي 1.403 انكستروم. ان معدل قيم الزوايا لحلقة البنزين وجدت مساوية لـ 119.98 درجة لطريقة نظرية الدالة الوظيفية للكثافة و مساوية لـ 120 درجة لطريقة هارترى- فوك حيث كانت هذه النتائج متوافقة مع القيم العيارية.

كما تم دراسة الطاقة الالكترونية وتوزيع الشحنات وطاقات اعلى مدار جزئي مملوء واطا مدار جزئي فارغ وفجوة الطاقة و عزم ثنائي القطب والمعلمات العالمية السبعة والاستقطاب وفرط الاستقطاب من الدرجة الاولى. ان الطاقة الالكترونية المحسوبة وجدت مساوية لـ 842.614348- و 953983. 837- بوحدات الهارترى لكل من نظرية الدالة الوظيفية للكثافة و طريقة هارترى - فوك على التوالي. وقد لوحظ بان هنالك عدم انتظام في توزيع الشحنات على الجزيئة ويرجع السبب في ذلك الى وجود قيمة لعزم ثنائي القطب حيث كانت مساوية لـ 3.3939 و 3.6661 بوحدات الديباي لكلا الطريقتين على التوالي. واستنادا الى قيمة فجوة الطاقة المحسوبة بطريقة نظرية الدالة الوظيفية للكثافة والمساوية لـ 8.326 بوحدات الالكترن فولت فان النظام يتمتع باستقرار كيميائي عالي اذا ما قورت بالقيمة المحسوبة باستخدام هارترى - فوك والمساوية لـ 4.522 بوحدات الالكترن فولت.

واخيرا تم دراسة وتحليل اطياف الاشعة تحت الحمراء واطياف رامان نظريا باستخدام برنامج GaussView 6 و برنامج Veda. وقد كانت النتائج المستحصلة من طريقة نظرية الدالة الوظيفية للكثافة متوافقة بصورة جيدة مع النتائج العالمية ولكلا التقنيتين.



جامعة كربلاء

كلية العلوم

قسم الفيزياء

دراسة نظرية للخصائص الالكترونية والطيفية لدايايل فثاليت

رسالة مقدمة الى مجلس كلية العلوم / جامعة كربلاء

كجزء من متطلبات نيل درجة الماجستير في علوم الفيزياء

كتبت بواسطة

شاكر عبد الرزاق غلام

بكالوريوس جامعة بغداد 1983

بإشراف

أ.م.د. محمد عبد الحسين الكعبي

شوال 1443 هـ

أيار 2022 م